CRB1 gene therapy coming of age: mechanistic insight and rAAV assays on mouse & human retinal organoid models

Buck, T.M.

Chapter 4

Human iPSC-Derived Retinas Recapitulate the Fetal CRB1 CRB2 Complex Formation and Demonstrate that Photoreceptors and Müller Glia Are Targets of AAV5

P.M. Quinn*, **T.M. Buck*,** A.A. Mulder, C. Ohonin, C.H. Alves, R.M. Vos, M. Białecka, T.v Herwaarden, E.H.C.v. Dijk, M. Talib, C. Freund, H.M.M. Mikkers, R.C. Hoeben, M.J. Goumans, C.J.F. Boon, A.J. Koster, S.M. Chuva de Sousa Lopes, C.R. Jost, and J. Wijnholds

***These authors contributed equally to this work (co-first authors)**

Stem Cell Reports, 2019,12(5),906-919

Abstract

Human retinal organoids from induced pluripotent stem cells (hiPSCs) can be used to confirm the localisation of proteins in retinal cell types and to test transduction and expression patterns of gene therapy vectors. Here, we compared the onset of CRB protein expression in human fetal retina to human iPSC-derived retinal organoids. We show that CRB2 protein precedes the expression of CRB1 in the developing human retina. Our data suggest the presence of CRB1 and CRB2 in human photoreceptors and Müller glial cells. Thus the fetal CRB complex formation is replicated in hiPSC-derived retina. *CRB1* patient iPSC retinal organoids showed disruptions at the outer limiting membrane as found in *Crb1* mutant mice. Furthermore, AAV serotype 5 (AAV5) is potent in infecting human Müller glial cells and photoreceptors in hiPSC-derived retinas and retinal explants. Our data suggest that human photoreceptors can be efficiently transduced by AAVs in the presence of photoreceptor segments.

INTRODUCTION

Mutations in the Crumbs homolog-1 (*CRB1*) gene are linked to an array of retinal dystrophies that exhibit high phenotypic variability and affect approximately 80,000 patients worldwide with an estimated prevalence in the US of 1/86,500 [1–3]. A meta-analysis has found that mutations in the *CRB1* gene account for 2.7% and 10.1% of autosomal recessive retinitis pigmentosa (RP) and Leber congenital amaurosis (LCA) cases, respectively [4]. LCA is an early onset disease with newborns being blind around birth. However, we are yet to understand the localisation of the CRB complex in early human fetal retinal development. No treatment is currently available for *CRB1*-associated retinal dystrophy in patients, but *proof-of-concept* gene supplementation studies have shown both morphological and functional rescue in *CRB1* retinitis pigmentosa mouse models [5]. A retrospective cohort study of patients with *CRB1*-associated retinitis pigmentosa has shown that gene therapeutic intervention is most likely required within the first three decades of life, but clinical endpoint criteria for a clinical trial need to be established from natural history studies [2]. Preclinical considerations to be evaluated include the choice of adeno-associated virus (AAV) serotype for delivery of the clinical vector, in terms of potency, tropism, safety and biodistribution.

Some retinal gene therapies are using a serotype of AAV as delivery vector in clinical trials [6–8] because they restrict vector tropism to specific retinal sub-populations, improve the efficiency of gene delivery, have low immunogenicity and long transgene expression. Cross-species differences in vector tissue tropism between mice and non-human primates have been previously highlighted and must be sufficiently addressed before moving towards clinical trials [9,10]. We previously showed proof of concept for *CRB1* gene therapy in *Crb1*-retinitis pigmentosa-like mice by subretinal application of an AAV9-CMV-*CRB2* gene therapy vector, thereby demonstrating the need of transgene expression in both photoreceptors and Müller glial cells [5]. Upon subretinal application, AAV9 and the AAV6 variant serotype ShH10Y445F are able to efficiently infect in mouse photoreceptors, Müller glial cells and retinal pigment epithelium, whereas AAV5 does not efficiently infect and express in mouse Müller glial cells [11,12]. AAV tropism differs between species, therefore the AAV serotype for clinical *CRB1*-gene therapy in both photoreceptors and Müller glial cells needs to be validated. AAV5 and AAV9 infect non-human primate rod and cone photoreceptors [13,14]. Human induced pluripotent stem cell (hiPSC)-derived retinal organoids, although *in vitro*, are a promising alternative or additional/pre-screening tool to animal models for evaluating transgene expression and biological activity [15]. As previously demonstrated by others and ourselves hiPSC-derived retinal organoids and photoreceptors are amenable for the testing of AAV serotype/promoter combinations [15–17]. However, for this purpose the hiPSC-derived retinal organoids should suitably recapitulate the human retina and the onset of expression of its proteins.

The core Crumbs complex in mammals is comprised of CRB1-3, PALS1 (also called MPP5), MUPP1 and PATJ. The prototypic CRB protein has a large extracellular domain with EGF-like domains and laminin-A globular domains adjacent to a single transmembrane domain. A short C-terminus of 37 amino acids contains a FERM protein-binding domain juxtaposing the single transmembrane domain. At the C-terminal end, there is a PDZ protein-binding motif of 4 amino acids (ERLI) that allow interaction with adaptor proteins such as PALS1 and PAR6 [18–21]. In non-human primates, CRB1 and CRB2 proteins localize to the subapical region adjacent to adherens junctions in Müller glial cells and photoreceptors [22]. Similarly, in two-days-old human adult cadaveric retina, both CRB1 and CRB2 are located at the subapical region in Müller glial cells. However, in photoreceptors, the CRB1 protein is detectable at the subapical region near to the outer limiting membrane, but CRB2 is not. Additionally, both CRB1 and CRB2 are detected at vesicles in the photoreceptor inner segments at a distance from the outer limiting membrane [5,23]. Thus far, the localisation of the CRB complex in early human fetal retinal development is unknown.

In this study, we show the recapitulation of the CRB complex between the human fetal retina and cultured hiPSC-derived retinal organoids. These studies highlight that CRB2, but not CRB1, is present at the subapical region in human fetal retina during the 1st trimester of pregnancy. CRB1 is expressed only at later time points from the 2nd trimester onwards concurring with the birth of differentiated cell types such as photoreceptors and Müller glial cells. These data suggest role(s) for CRB2 but not CRB1 in the 1st trimester in the earliest human retinal radial glial progenitor cells. The data also suggest that *CRB1* patient iPSC-derived retinal organoids develop a retinal phenotype as found in *Crb1*^{KO} and *Crb1*$^{KO/C249W}$ mice [24–26].

Additionally, we show higher efficacy of AAV5 and ShH10Y445F over AAV9 serotypes for infection of photoreceptors in cultured human donor retinal explants. We also show the preference of AAV5 and ShH10Y445F over AAV9 to infect Müller glial cells in hiPSC-derived retinal organoids. Overall, our results suggest that the AAV5 serotype combined with CMV-promoter mediated expression is suitable for gene therapy of *CRB* genes into human Müller glial cells and rod and cone photoreceptors.

RESULTS

Retinal architecture in the human fetal retina and iPSC retinal organoids

The human fetal retina, as it transitions from the 1st to the 2nd trimester of pregnancy, gives rise to all adult retinal cell types as the retina moves from a mitotic to post-mitotic state [27]. We examined 1st (week 11-13) and 2nd Trimester (weeks 16-18) fetal retina and compared these with early (differentiation day 30 (DD30)) and late (DD120 -DD240) healthy hiPSC retinal organoids. The retinal architecture in the human fetal retina recapitulated the retinal architecture as found in hiPSC retinal organoids (Figures S1 and S2).

The CRB complex in the human fetal retina and iPSC retinal organoids

We undertook immunohistochemistry studies to delineate the onset of expression of CRB1 and CRB2 in 1st and 2nd trimester human fetal retina and in early and late stage differentiated retinal organoids. In week 9 human fetal retina we did not detect the typical puncta-like CRB1$^+$ immunostaining at the subapical region adjacent to the adherence junction marker β-catenin (Figures S3A-C). However, at week 11 we observed a gradient of CRB1 immunostaining located at the outer limiting membrane (OLM) (Figure 1A). In week 9 and 11 the human fetal retina stained positive for CRB2 at the subapical region adjacent to the adherence junctions as marked by anti-p120-catenin (Figures 1B, S3D-F). Furthermore, in the 1st trimester fetal retina at week 9 (Figures S3G-I), we found PATJ at the OLM and additionally in a subset of anti-Ki67$^+$ cells; this was also seen in the developing mouse retina [28]. In week 19 the human fetal retina expressed CRB1 (Figure 1E) and CRB2 (Figure 1F) with their prototypic puncta immunostaining pattern. Immunostaining for CRB complex members PALS1, MUPP1, PAR3 and the adherens junction markers β-catenin, p120-catenin and N-cadherin were detected in both 1st and 2nd trimester human fetal retina (Figure 1).

Similarly, In DD28 and DD80 retinal organoids we did not detect typical CRB1$^+$ puncta-like immunostaining (Figures 1I and S3J). Its family member CRB2 was present at DD28 and DD80 (Figures 1J and S3K). PALS1 and MUPP1 were present at the subapical region in DD28 hiPSC-derived retinal organoids (Figures S3L and S3M). Moreover, in retinal organoids at DD30 (Figures S3N-P) we found PATJ at the OLM and additionally in a subset of anti-Ki67$^+$ cells. However, a typical and clear puncta-like staining pattern for CRB1 was detected at DD160 subapical of adherens junctions marker β-catenin (Figure 1K). CRB complex members CRB2, PALS1, MUPP1 and PAR3 and adherens junction markers p120-catenin and N-cadherin were also detected in DD160 retinal organoids (Figures 1L-O). CRB1 and CRB2 localisation in retinal organoids was also confirmed in two other hiPSC lines: LUMC0080iCTRL12 (Figures S3Q, S3R, S3S), LUMC0044iCTRL44 (Figures 5E-H, 6E-H).

Ultra-localisation of CRB1 and CRB2 in the human fetal retina and in iPSC retinal organoids

We performed immuno-EM studies to analyse at ultra-high resolution the localisation of CRB1 and CRB2 in PRCs and MGCs in 1st and 2nd trimester human fetal retina and in retinal organoids. Immuno-EM for CRB1 in the 1st trimester fetal retina showed occasional and limited staining at putative inner segments (Figure 2A) and apical villi (Figure 2B) of radial glial progenitor cells. However, in the 2nd trimester CRB1 labelling could be clearly detected at the subapical region adjacent to adherens junctions between putative photoreceptor inner segments (Figure 2C) and in the apical villi of radial glial progenitor cells/ MGCs (Figure 2D). Immuno-EM for CRB2 showed pronounced labelling in 1st (Figures 3E and 3F) and 2nd trimester (Figures 2G and 2H) fetal retina. CRB2 labelling localised at the plasma membrane and at the subapical region adjacent to adherens junctions between putative photoreceptor

inner segments (Figures 2E and 2G) and in the apical villi of radial glial progenitor cells/ MGCs (Figures 2F and 2H).

Similarly to 1st trimester human fetal retina, immuno-EM performed on retinal organoids showed sporadic and limited CRB1 labelling at the subapical region adjacent to adherens junctions between putative photoreceptor inner segments (Figure 3A) and in the apical villi of radial glial progenitor cells/ MGCs (Figure 3B) in early retinal organoids. However, in late retinal organoids CRB1 labelling localised at the plasma membrane and at the subapical region adjacent to adherens junctions between putative photoreceptor inner segments (Figure 3C) and in the apical villi of radial glial progenitor cells/ MGCs (Figure 3D). Immuno-EM for CRB2 showed pronounced labelling in early (Figures 3E and 3F) and late (Figures 3G and 3H) retinal organoids. CRB2 labelling localised at the plasma membrane and at the subapical region adjacent to adherens junctions between putative photoreceptor inner segments (Figures 3E and 3G) and in the apical villi of radial glial progenitor cells/ MGCs (Figures 3F and 3H).

Taken together, these data suggest that CRB1 is not required for the localisation of CRB2, PALS1, MUPP1 or PATJ in the first trimester of human retinal development. The onset of CRB protein expression in human fetal retina is recapitulated in retinal organoids.

Disruptions at the outer limiting membrane in retinal organoids from CRB1 retinitis pigmentosa (RP) patients

We generated three hiPSC lines (LUMC0116iCRB; LUMC0117iCRB; LUMC0128iCRB) from *CRB1* RP patients. As with healthy iPSCs (Figure S4A), patient iPSCs were validated via immunostaining with pluripotent and germ layer markers (Figure S4B). LUMC0116iCRB has c.3122T>C p.(Met1041Thr) homozygote missense mutations. LUMC0117iCRB has 2983G>T p.(Glu995*) and c.1892A>G, p.(Tyr631Cys) mutations. LUMC0128iCRB has c.2843G>A p.(Cys948Tyr) and c.3122T>C p.(Met1041Thr) missense mutations. The *CRB1* gene mutations were re-confirmed in the established iPSCs (Figure S4C).

CRB1 patient iPSCs were able to differentiate to DD180 retinal organoids and were compared to healthy retinal organoids (Figure 4). The patient retinal organoids had $pH3^+$ mitotic cells apically at the OLM, with $Ki67^+$ cycling cells less tightly restricted to the middle of the NBL (Figure 4I, M, Q). The *CRB1* patient iPSCs retinal organoids developed all three retinal layers: a GCL marked by $Tuj1^+$ dendrites (Figure 4J, N, R), a NBL marked by $SOX9^+$ retinal progenitor cells/MGCs (Figure 4K, O, S) and an ONL marked by $recoverin^+$ PRCs (Figure 4L, P, T). However, frequent ectopic cells were found above the OLM (Figure 4I-T). We observed many areas of funnel-shaped outward protruding $recoverin^+$ PRCs (Figures 4L, P, T) and sporadically $SOX9^+$ cells above the OLM (Figure 4O).

All retinal organoids from the three different *CRB1* patient lines developed small but frequent disruptions of CRB complex members at the OLM that were not detected in control lines (Figure 5). The adherens junction proteins N-Cadherin, p120-catenin, β-catenin and the subapical region proteins CRB2, PALS1, PAR3, MUPP1 were localized as in healthy retinal organoids at DD180 (Figure 5). Interestingly, CRB1 variant protein localized similar as the wild type CRB1 protein at the subapical region above the adherens junctions but showed a curved and broadened expression pattern (Figure 5I, M, Q, U) compared to the healthy control lines (Figure 5A, E). CRB1 variant protein was also mislocalized in the apical area of the NBL and in the ONL (Figure 5I, M,Q). The mislocalized PRCs above the OLM resided at areas of OLM disruptions (Figure 5V, W, X). In conclusion, the data from *CRB1* patient hiPSC retinal organoids suggest a retinal degeneration phenotype similar as previously found in mice lacking CRB1 or expressing variant CRB1^{C249W} [24–26].

Transduction of human iPSC retinal organoids with AAV5, AAV9 and ShH10Y445F

Human iPSC-derived retinal organoids are a promising tool for evaluating transgene expression and biological activity [15]. We have shown the need in *Crb1*-retinitis pigmentosa like mice to direct *CRB* gene therapy to both photoreceptors and Müller glial cells [5]. Choosing the optimal promoter and AAV serotype for the therapeutic vector is therefore crucial to achieving expression in photoreceptors and Müller glial cells. Here, we transduced the hiPSC-derived retinal organoids with AAV9-CMV-*GFP*, AAV5-CMV-*GFP*, ShH10Y445F-CMV-*GFP* and ShH10Y445F-RLBP1-*GFP* at 10^{10} genome copies (gc). The CMV promoter drives expression of GFP in multiple cell types, whereas the hRLBP1 promoter drives expression in Müller glial cells and retinal pigment epithelial cells [11]. When analysed at the same laser intensity settings (Figures S5A-D) AAV5-CMV-*GFP*, ShH10Y445F-CMV-*GFP* and ShH10Y445F-hRLBP1-*GFP* significantly outperformed AAV9-CMV-*GFP* at transducing DD220 hiPSC-derived retinal organoids collected 14 days after infection (Figures 6E and 6F). We quantified both the number of GFP$^+$ cells per total cells (Figure 6E) and the mean grey value (Figure 6F) for each vector. The GFP$^+$ nuclei were mainly located in the inner retina and exhibited radial projections. The GFP$^+$ nuclei co-localised with anti-LHX2 (Figures 6A-D, inserts) and anti-SOX2 (Figures S5E-H and S5E'-H') both transcription factors required for Müller glial cell development. Further proof of Müller glial specific transduction is also seen with the use of ShH10Y445F-RLBP1-*GFP* (Figure 6D) which drives GFP in Müller glial cells in rat and mouse retinas [11,29]. We additionally stained with anti-recoverin and found occasional co-localisation between the photoreceptor marker and GFP$^+$ nuclei (Figures S5I-L and S5I'-L'). In conclusion, these results indicate that AAV5 and ShH10Y445F serotypes are more potent transducers of Müller glial cells than AAV9 in hiPSC-derived retinal organoids.

Transduction of adult post-mortem human retinal explants with serotypes AAV5, AAV9 and ShH10Y445F

To verify the results of our transduction studies on hiPSC-derived retinal organoids we also tested AAV9-, AAV5- and ShH10Y445F-CMV-*GFP* on human adult retinal explants. Initially, a titration study for AAV9 (Figure S6A-C), AAV5 (Figure S6D-F), and ShH10Y445F (Figure S6G-I) was undertaken to determine what genome copies (gc) level is required to infect photoreceptors and Müller glial cells efficiently. Analysis for total infection (Figures S6P and S6Q), infection per retinal layer (Figures S6R and S6S) and tropism (Figure S6T) in donor 1 indicated $3x10^{10}$ gc as a suitable level. Similar transduction patterns were found in donor 1 (Figures 6H-K, 6L-N, S6B, D, G), donor 2 (Figures S6J-L) and donor 3 (Figures S6M-O) at $3x10^{10}$ gc. With individual analysis for total infection (Figures S6U, S6V, S6Y and S6Z), infection per retinal layer (Figures S6W and S6AA) and tropism (Figures S6X and S6BB) also done for donors 2 and 3 at $3x10^{10}$ gc. Donors 1-3 had similar retinal layer thickness (Figure S6CC) and cells per retinal layer (Figure S6DD). In the INL, GFP co-labelled with Müller glial cell marker anti-SOX9 (Figures 6G-J); and in the ONL, GFP co-labelled with photoreceptor marker anti-recoverin (Figures 6K-N). When analysing donors 1-3 together, AAV5 showed the higher efficacy of transducing retinal cell types than AAV9 (14±5% vs 3±1%; Figure 6O), and AAV5 and ShH10Y445F showed higher potency in transduction of photoreceptors in the ONL than AAV9 (11±3% and 5±1% vs 3±1%; Figures 6P and 6Q). Interestingly, we noticed that the photoreceptors of cadaveric human retinal explants were only efficiently infected by AAV9 (Figure S7A, B) or AAV5 (Figure S7C) or ShH10Y445F (Figure S7D) in the presence of intact photoreceptor segments (Figure S7E-G). This suggests an important role for the segments in the photoreceptor uptake of AAV particles. In conclusion, transduction of AAV serotypes in human cadaveric retina was more successful at targeting both photoreceptors and Müller glial cells than in hiPSC-derived retinal organoids. AAV5 at $3x10^{10}$ gc significantly outperformed AAV9 in the transduction of photoreceptor cells.

CRB2 is located in the apical membrane of iPSC-derived and fetal retinal pigment epithelium

CRB2 but not CRB1 immunostaining was detected in 1st trimester human fetal RPE (Figures S3D'-F'). This was confirmed by immuno-EM in 1st and 2nd trimester human fetal RPE (Figures 7A and 7B). CRB2 labelling was located above the adherens junctions at and above the tight junctions in the apical membrane and microvilli of human fetal RPE. Spheroids of hiPSC-derived RPE are also generated during the differentiation method used [15,30,31]. These RPE spheroids initially attach to the periphery of the retinal organoids but can detach during culturing (Figures 7C, 7D and 7D'). CRB1 could not be detected apically of β-catenin (Figure 7C) in hiPSC-derived RPE, but CRB2 was found apically of the adherens junction marker p120-catenin in DD160 hiPSC-derived RPE (Figure 7D). This pattern of localisation was also found in hiPSC-derived RPE derived from hiPSC lines LUMC0080iCTRL12

(Figures 7E and S7F) and LUMC0044iCTRL44 (Figures 7G and 7H). Immuno-EM of iPSC-derived RPE confirmed the apical staining for CRB2 above adherens junctions at and above the tight junctions in the apical membrane and microvilli. Aspecific staining was detected within melanin granules due to the presence of endogenous peroxidase in these structures (Figures 7I and 7I'). Electron microscopy of hiPSC-derived RPE also showed the presence of melanosomes with pigments, basally located mitochondria and basement membrane (Figure 7J, insert) and fibrous long-spacing collagen (FLSC) (Figures 7J and 7J'). RPE cells were also infected by AAV9, AAV5 and ShH10Y445F (Figures S7H-K).

DISCUSSION

In this study, we showed (i) that in human fetal retina during the 1st trimester of pregnancy CRB2 is the predominant CRB family member in radial glial progenitor cells. And that CRB1 onset of expression at the subapical region coincides with the maturation of the retina during the 2nd trimester. (ii) CRB2 but not CRB1 is expressed in the fetal RPE. (iii) The onset of CRB protein expression in human fetal retina and RPE is recapitulated in hiPSC-derived retinal organoids and RPE. (iv) *CRB1* RP patient retinal organoids develop disruptions at the OLM with misplaced photoreceptors. (v) AAV5 and ShH10Y445F serotypes are more potent than AAV9 serotype in infecting cultured retinal organoids. (vi) AAV5-CMV-*GFP* is more efficient than AAV9-CMV-*GFP* to express GFP in PRCs in cultured human donor retinal explants. (vii) Human PRCs are efficiently transduced only in the presence of photoreceptor segments.

In the human fetal retina, we found that CRB2 is the predominant CRB effector protein in the 1st trimester of pregnancy. *CRB2* is a gene expressed in several tissues, including the cerebral cortex [32], with a crucial role during early development in both mice and humans. Mice lacking *Crb2* are embryonic lethal with a critical role for the CRB2 protein during gastrulation in the epithelial-to-mesenchymal transition [33]. CRB2 protein variants in humans have been linked to a syndromic phenotype causing kidney and brain dysfunctions and lethality [34,35] as well as to retinitis pigmentosa [36]. In the 2nd trimester, CRB1 and CRB2 localised at the subapical region in apical villi of radial glial progenitor cells/MGCs and at the subapical region above the adherens junctions in the inner segments of PRCs. During the 2nd trimester, the retina undergoes the birth of all adult cell types, and the retina is transitioning from a mitotic to post-mitotic state [27,37]. Retinal organoids go from an early highly-cell-cycling state, in which Ki67 marks the entire NBL at DD28, towards a moderate-cell-cycling state, in which Ki67 becoming restricted to the mid-NBL at DD120.

Interestingly, here we showed that the onset of CRB1 protein expression coincided with the maturation of the retinal organoids, and this finding is recapitulated in the human fetal retina. In early-stage retinal organoids, we found as in the 1st trimester fetal retina CRB2 but little CRB1 protein expression at the subapical region. In later stage hiPSC-derived retinal organoids we found CRB2 and CRB1 protein expression at the subapical region as in 2nd

trimester fetal retina. We also found a recapitulation of CRB2 expression when comparing 1st trimester fetal RPE with hiPSC-derived RPE.

We present here the generation and characterization of *CRB1*-patient-derived hiPSCs differentiated to retinal organoids. We demonstrate that patient retinal organoids give rise to a morphological significant phenotype even though variant CRB1 protein and its interaction partners (MUPP1, PALS1, CRB2) are detected at the OLM. The data suggests disruptions at the OLM resulting in loss of adhesion between photoreceptors and Müller glial cells. Decreased levels of CRB1 and CRB2 proteins at the OLM exacerbated retinal degeneration in mouse models [28,38,39]. Also, the volcanic-like cell protrusions and OLM disruptions in the patient retinal organoids show striking similarities to the morphological phenotype found in 3 month-old $Crb1^{KO}$ and 8 month-old $Crb1^{KO/C249W}$ RP mice [24–26]. Further studies are needed to elucidate the underlying effects of the variant CRB1 proteins on protein-protein interactions and downstream cell signalling pathways.

We hypothesise that retinal organoids could be a good model for evaluating transgene expression and biological activity due to their close mimicking of human fetal retinal development [15]. Our transduction studies on cadaveric human retinal explants showed a higher potency for AAV5 over AAV9 for transduction of photoreceptors. Also, the data suggest the higher efficacy of AAV5-CMV-*GFP* than AAV9-CMV-*GFP* or ShH10Y445F-CMV-*GFP* to express in PRCs and MGCs. In the absence of photoreceptor segments in the human retinal explants, AAV5-CMV-*GFP,* ShH10Y445F-CMV-*GFP* and AAV9-CMV-*GFP* showed higher efficacy to express in MGCs than in PRCs. The latter tropism and expression potency data in cultured cadaveric human retinal explants are reproduced in retinal organoids that recapitalise 2nd trimester fetal retina.

Previous subretinal injection studies in which AAV5 was administered in mice at postnatal day 0 (P0) or 30 (P30) have shown preferred transduction of P0 cone PRC and MGCs but only of P30 rod and cone PRCs [40]. We hypothesise that this preference in transduction patterns of PRC and MGCs in immature versus mature retina is due to the presence or absence of matured photoreceptor segments. In mice, photoreceptor segments seem to be required for the efficient transduction of photoreceptor cells with AAV vectors [41]. A very interesting and clinically relevant finding is that photoreceptors in cultured cadaveric human retinal explants are only efficiently transduced when they have photoreceptor segments. Retinal organoids represent immature fetal retina that contain PRCs but with yet very immature segments. We hypothesise that PRCs are transduced by AAV5, AAV9 and ShH10Y445F once the PRC segments are formed in sufficient number and size. In the absence of PRC segments, however, there is increased bioavailability of AAV vectors to target less abundant/preferred receptors for AAV uptake, e.g. on MGCs. Interestingly, dependency on the presence of photoreceptor segments for photoreceptor transduction was observed for all three AAV serotypes (AAV5, AAV9 and ShH10Y445F), suggesting a putative common

mechanism of active AAV uptake into photoreceptors. The inner segments are a putative site of receptor-dependent or independent clathrin- and caveolae-mediated endocytosis [42].

Our data suggest that for clinical gene therapy with AAV5, AAV9 or ShH10Y445F the target PRCs should have intact photoreceptors to become efficiently transduced. It also implies that the AAV vector particles should be able to reach the PRC segments during clinical surgical application. This condition of accessibility of PRC inner segments in human retina *in vivo* is met upon subretinal injection as suggested by AAV5 or AAV9 infection of PRCs in non-human-primate retinas [14,43]. Our mice lacking CRB1 as well as the mice with reduced levels of CRB2 showed a compromised outer limiting membrane. We further hypothesise from our previous studies in mice that the retinas of human patients with loss of CRB1, or expressing non-functional CRB1 variants, have a compromised outer limiting membrane that allows increased passage of AAV viral particles across the adherence junctions to reach the AAV-receptor molecules on MGCs [44].

MATERIALS AND METHODS

Experimental Procedures

See further details in the Supplemental Experimental Procedures.

Fetal human retinal tissue

The use and collection of the material was approved by the Medical Ethics Committee of the Leiden University Medical Center (P08.087).

Adult human retinal tissue

Tissue was collected in agreement with the guidelines of the ethics committee of the LUMC. Informed consent was obtained on the basis of the Declaration of Helsinki (World Medical Association).

Cell Culture and Retinal Organoid Differentiation

Human iPSCs (LUMC0004iCTRL10 (Dambrot et al., 2014), LUMC0044iCTRL44 (Chen et al., 2017), LUMC0080iCTRL12 (Figure S4A), LUMC0116iCRB09, LUMC0117iCRB01, LUMC0128iCRB01 (Figure S4B)) were maintained on Matrigel (BD) coated plates in mTeSR medium (STEMCELL Technologies) and passaged mechanically. Retinal organoid differentiation was carried out as previously reported (Quinn et al., 2018a; Zhong et al., 2014).

Electron microscopy

Immuno-electron microscopy was performed as previously described (Klooster et al., 2011). In brief, Sections were incubated with first antibody for 48 h, then incubated with appropriate secondary peroxidise anti-peroxidase (PAP) for 2h, then developed in a 2,2-

diaminobenzidine solution for 4 min and then the gold substitute silver peroxidise method applied.

Generation and purification of the viral vectors

The pAAV2-*eGFP* plasmids were generated previously and consist of the flanking inverted terminal repeats (ITRs) of AAV2, the full-length CMV promoter, or the human RLBP1 promoter, the *eGFP* cDNA, the Woodchuck posttranscriptional regulatory element (WPRE) and the bovine growth hormone poly(A) (bGHpoly(A) (Aartsen et al., 2010; Alves et al., 2014b; Pellissier et al., 2014a).

In vitro transduction of human donor retina and human induced pluripotent stem cell derived retinal organoids

In vitro transduction protocols for 1) human donor retina and 2) hiPSC-derived retinal organoids have been described (Buck et al., 2018; Quinn et al., 2018a).

Statistical method

All statistical analyses were performed using GraphPad Prism version 7 (GraphPad Software). All values are expressed as mean ± SEM. Multiple t-tests were performed with the analysed number of samples indicated in the figure legends. Immunohistochemistry was performed on iPSC-derived retinal organoids from 3 independent healthy and 3 independent *CRB1*-patient iPSC lines from 2 or more differentiations, with 3-6 sections examined per organoid. Immunohistochemistry was performed on at least 2 independent human fetal eyes per time point, with 3-6 sections examined per eye. Immuno-EM was performed on at least 2 independent human fetal eyes, iPSC-derived retinal organoids and RPE for each time point. For AAV transduction studies between 3-6 different sections from at least three different human donor retina or hiPSC-derived retinal organoids (1-2 organoids from 2 independent differentiations analysed) were used for quantification. Between 3-5 images per organoid and 10 images per adult donor retina were analysed.

Author contributions

P.M.Q., T.M.B. and J.W. conceived and designed the experiments. P.M.Q., T.M.B., C.O., C.H.A., A.A.M., performed the experiments. R.V. produced virus stocks. M.B., T.v.H., E.H.C.v.D., M.T., collected study material. H.M.M., C.F., R.C.H., M-J.G., C.J.F.B., A.J.K. and S.M.C.d.S.L. provided study material and/or access to facilities. P.M.Q. and T.M.B. assembled data. P.M.Q., T.M.B., A.A.M., C.R.J. and J.W. analysed and interpreted the data. P.M.Q., T.M.B. and J.W. wrote the manuscript. All authors reviewed the manuscript. J.W. provided funding acquisition, supervision and final approval of manuscript.

Acknowledgments

The Wijnholds Laboratory would like to thank Yacintha van Doorn and Hind Almushattat for differentiation of retinal organoids, André Le Bivic for providing PATJ antibodies, Maaike Nieveen and Fang Wang for collecting study materials, Annelies van der Laan and Joop Wiegant from the LUMC microscope facility, and Anke 't Jong from the LUMC iPSC facility for advice. We would like to thank the abortion clinic Gynaikon in Rotterdam for the collection of the fetal material. We would also like to thank all our supporters, which include the Foundation Fighting Blindness USA (TA-GT-0313-0607-NIN and TA-GT-0715-0665-LUMC), the Netherlands Organization for Health Research and Development (ZonMw grant 43200004), the Curing Retinal Blindness Foundation (CRBF), Stichting Retina Nederland Fonds, Landelijke Stichting voor Blinden en Slechtzienden (LSBS), Rotterdamse Stichting Blindenbelangen (RSB), Stichting Blindenhulp, Stichting Blinden-Penning, Algemene Nederlandse Vereniging ter Voorkoming van Blindheid (ANVVB), Gelderse Blinden Stichting (GBS), and MaculaFonds. The LUMC is the holder of patent number PCT/NL2014/050549, which describes the potential clinical use of CRB2; JW is listed as inventor on this patent, and JW is an employee of the LUMC. The authors declare that the research was conducted without any commercial or financial relationships that could be construed as a potential conflict of interest.

REFERENCES

1. Alves, C.H.; Pellissier, L.P.; Wijnholds, J. The CRB1 and adherens junction complex proteins in retinal development and maintenance. *Prog. Retin. Eye Res.* **2014**, *40*, 35–52.
2. Talib, M.; van Schooneveld, M.J.; van Genderen, M.M.; Wijnholds, J.; Florijn, R.J.; ten Brink, J.B.; Schalij-Delfos, N.E.; Dagnelie, G.; Cremers, F.P.M.; Wolterbeek, R.; et al. Genotypic and Phenotypic Characteristics of CRB1-Associated Retinal Dystrophies: A Long-Term Follow-up Study. *Ophthalmology* **2017**, *124*, 884–895.
3. Stone, E.M.; Andorf, J.L.; Whitmore, S.S.; DeLuca, A.P.; Giacalone, J.C.; Streb, L.M.; Braun, T.A.; Mullins, R.F.; Scheetz, T.E.; Sheffield, V.C.; et al. Clinically Focused Molecular Investigation of 1000 Consecutive Families with Inherited Retinal Disease. *Ophthalmology* **2017**, *124*, 1314–1331.
4. Bujakowska, K.; Audo, I.; Mohand-Saïd, S.; Lancelot, M.-E.; Antonio, A.; Germain, A.; Léveillard, T.; Letexier, M.; Saraiva, J.-P.; Lonjou, C.; et al. CRB1 mutations in inherited retinal dystrophies. *Hum. Mutat.* **2012**, *33*, 306–315.
5. Pellissier, L.P.; Quinn, P.M.; Henrique Alves, C.; Vos, R.M.; Klooster, J.; Flannery, J.G.; Alexander Heimel, J.; Wijnholds, J. Gene therapy into photoreceptors and Müller glial cells restores retinal structure and function in CRB1 retinitis pigmentosa mouse models. *Hum. Mol. Genet.* **2015**, *24*, 3104–3118.
6. Reichel, F.F.; Peters, T.; Wilhelm, B.; Biel, M.; Ueffing, M.; Wissinger, B.; Bartz-Schmidt, K.U.; Klein, R.; Michalakis, S.; Fischer, M.D.; et al. Humoral Immune Response After Intravitreal But Not After Subretinal AAV8 in Primates and Patients. *Invest. Ophthalmol. Vis. Sci.* **2018**, *59*, 1910–1915.
7. Maguire, A.M.; Simonelli, F.; Pierce, E.A.; Pugh, E.N.; Mingozzi, F.; Bennicelli, J.; Banfi, S.; Marshall, K.A.; Testa, F.; Surace, E.M.; et al. Safety and efficacy of gene transfer for Leber's congenital amaurosis. *N. Engl. J. Med.* **2008**, *358*, 2240–2248.
8. MacLaren, R.E.; Groppe, M.; Barnard, A.R.; Cottriall, C.L.; Tolmachova, T.; Seymour, L.; Reed Clark, K.; During, M.J.; Cremers, F.P.M.; Black, G.C.M.; et al. Retinal gene therapy in patients with choroideremia: Initial findings from a phase 1/2 clinical trial. *Lancet* **2014**, *383*, 1129–1137.
9. Asokan, A.; Schaffer, D. V; Jude Samulski, R. The AAV Vector Toolkit: Poised at the Clinical Crossroads. *Mol. Ther.* **2012**, *20*, 699–708.
10. Ramachandran, P.S.; Lee, V.; Wei, Z.; Song, J.Y.; Casal, G.; Cronin, T.; Willett, K.; Huckfeldt, R.; Morgan, J.I.W.; Aleman, T.S.; et al. Evaluation of Dose and Safety of AAV7m8 and AAV8BP2 in the Non-Human Primate Retina. *Hum. Gene Ther.* **2017**, *28*, 154–167.

11. Pellissier, L.P.; Hoek, R.M.; Vos, R.M.; Aartsen, W.M.; Klimczak, R.R.; Hoyng, S.A.; Flannery, J.G.; Wijnholds, J. Specific tools for targeting and expression in Müller glial cells. *Mol. Ther. — Methods Clin. Dev.* **2014**, *1*, 14009.
12. Aartsen, W.M.; van Cleef, K.W.R.R.; Pellissier, L.P.; Hoek, R.M.; Vos, R.M.; Blits, B.; Ehlert, E.M.E.E.; Balaggan, K.S.; Ali, R.R.; Verhaagen, J.; et al. GFAP-driven GFP expression in activated mouse Müller glial cells aligning retinal blood vessels following intravitreal injection of AAV2/6 vectors. *PLoS One* **2010**, *5*, e12387.
13. Vandenberghe, L.H.; Bell, P.; Maguire, A.M.; Xiao, R.; Hopkins, T.B.; Grant, R.; Bennett, J.; Wilson, J.M. AAV9 targets cone photoreceptors in the nonhuman primate retina. *PLoS One* **2013**, *8*, e53463.
14. Boye, S.E.; Alexander, J.J.; Boye, S.L.; Witherspoon, C.D.; Sandefer, K.J.; Conlon, T.J.; Erger, K.; Sun, J.; Ryals, R.; Chiodo, V.A.; et al. The Human Rhodopsin Kinase Promoter in an AAV5 Vector Confers Rod- and Cone-Specific Expression in the Primate Retina. *Hum. Gene Ther.* **2012**, *23*, 1101–1115.
15. Quinn, P.M.; Buck, T.M.; Ohonin, C.; Mikkers, H.M.M.M.; Wijnholds, J. Production of iPS-derived human retinal organoids for use in transgene expression assays. In *Methods in Molecular Biology*; Humana Press Inc., 2018; Vol. 1715, pp. 261–273.
16. Wiley, L.A.; Burnight, E.R.; Drack, A. V.; Banach, B.B.; Ochoa, D.; Cranston, C.M.; Madumba, R.A.; East, J.S.; Mullins, R.F.; Stone, E.M.; et al. Using Patient-Specific Induced Pluripotent Stem Cells and Wild-Type Mice to Develop a Gene Augmentation-Based Strategy to Treat *CLN3* -Associated Retinal Degeneration. *Hum. Gene Ther.* **2016**, *27*, 835–846.
17. Khabou, H.; Garita-Hernandez, M.; Chaffiol, A.; Reichman, S.; Jaillard, C.; Brazhnikova, E.; Bertin, S.; Forster, V.; Desrosiers, M.; Winckler, C.; et al. Noninvasive gene delivery to foveal cones for vision restoration. *JCI insight* **2018**, *3*.
18. Bulgakova, N.A.; Knust, E. The Crumbs complex: from epithelial-cell polarity to retinal degeneration. *J. Cell Sci.* **2009**, *122*, 2587–96.
19. Bachmann, A.; Schneider, M.; Theilenberg, E.; Grawe, F.; Knust, E. Drosophila Stardust is a partner of Crumbs in the control of epithelial cell polarity. *Nature* **2001**, *414*, 638–643.
20. Lemmers, C.; Michel, D.; Lane-Guermonprez, L.; Delgrossi, M.-H.; Médina, E.; Arsanto, J.-P.; Bivic, A. Le CRB3 Binds Directly to Par6 and Regulates the Morphogenesis of the Tight Junctions in Mammalian Epithelial Cells. *Mol. Biol. Cell* **2004**, *15*, 1324.
21. Roh, M.H.; Makarova, O.; Liu, C.-J.; Shin, K.; Lee, S.; Laurinec, S.; Goyal, M.; Wiggins, R.; Margolis, B. The Maguk protein, Pals1, functions as an adapter, linking mammalian homologues of Crumbs and Discs Lost. *J. Cell Biol.* **2002**, *157*, 161–72.
22. Quinn, P.M.; Mulder, A.A.; Henrique Alves, C.; Desrosiers, M.; de Vries, S.I.; Klooster, J.; Dalkara, D.; Koster, A.J.; Jost, C.R.; Wijnholds, J. Loss of CRB2 in Müller glial cells modifies a CRB1-associated retinitis pigmentosa phenotype into a Leber congenital amaurosis phenotype. *Hum. Mol. Genet.* **2019**, *28*, 105–123.
23. Pellissier, L.P.; Lundvig, D.M.S.; Tanimoto, N.; Klooster, J.; Vos, R.M.; Richard, F.; Sothilingam, V.; Garcia Garrido, M.; Le Bivic, A.; Seeliger, M.W.; et al. CRB2 acts as a modifying factor of CRB1-related retinal dystrophies in mice. *Hum. Mol. Genet.* **2014**, *23*, 3759–3771.
24. van de Pavert, S.A.; Sanz, A.S.; Aartsen, W.M.; Vos, R.M.; Versteeg, I.; Beck, S.C.; Klooster, J.; Seeliger, M.W.; Wijnholds, J. Crb1 is a determinant of retinal apical Müller glia cell features. *Glia* **2007**, *55*, 1486–1497.
25. van de Pavert, S.A.; Kantardzhieva, A.; Malysheva, A.; Meuleman, J.; Versteeg, I.; Levelt, C.; Klooster, J.; Geiger, S.; Seeliger, M.W.; Rashbass, P.; et al. Crumbs homologue 1 is required for maintenance of photoreceptor cell polarization and adhesion during light exposure. *J. Cell Sci.* **2004**, *117*, 4169–4177.
26. van de Pavert, S.A.; Meuleman, J.; Malysheva, A.; Aartsen, W.M.; Versteeg, I.; Tonagel, F.; Kamphuis, W.; McCabe, C.J.; Seeliger, M.W.; Wijnholds, J. A single amino acid substitution (Cys249Trp) in Crb1 causes retinal degeneration and deregulates expression of pituitary tumor transforming gene Pttg1. *J. Neurosci.* **2007**, *27*, 564–573.
27. Provis, J.M.; van Driel, D.; Billson, F.A.; Russell, P. Development of the human retina: patterns of cell distribution and redistribution in the ganglion cell layer. *J. Comp. Neurol.* **1985**, *233*, 429–451.
28. Alves, C.H.; Sanz, A.S.; Park, B.; Pellissier, L.P.; Tanimoto, N.; Beck, S.C.; Huber, G.; Murtaza, M.; Richard, F.; Sridevi Gurubaran, I.; et al. Loss of CRB2 in the mouse retina mimics human retinitis pigmentosa due to mutations in the CRB1 gene. *Hum. Mol. Genet.* **2013**, *22*, 35–50.
29. Klimczak, R.R.; Koerber, J.T.; Dalkara, D.; Flannery, J.G.; Schaffer, D. V. A novel adeno-associated viral variant for efficient and selective intravitreal transduction of rat Müller cells. *PLoS One* **2009**, *4*, e7467.
30. Zhong, X.; Gutierrez, C.; Xue, T.; Hampton, C.; Vergara, M.N.; Cao, L.-H.; Peters, A.; Park, T.S.; Zambidis, E.T.; Meyer, J.S.; et al. Generation of three-dimensional retinal tissue with functional photoreceptors from human iPSCs. *Nat. Commun.* **2014**, *5*, 4047.
31. Liu, S.; Xie, B.; Song, X.; Zheng, D.; He, L.; Li, G.; Gao, G.; Peng, F.; Yu, M.; Ge, J.; et al. Self-Formation of RPE Spheroids Facilitates Enrichment and Expansion of hiPSC-Derived RPE Generated on Retinal Organoid Induction Platform. *Invest. Ophthalmol. Vis. Sci.* **2018**, *59*, 5659–5669.
32. Dudok, J.J.; Murtaza, M.; Henrique Alves, C.; Rashbass, P.; Wijnholds, J. Crumbs 2 prevents cortical abnormalities in mouse dorsal telencephalon. *Neurosci. Res.* **2016**, *108*, 12–23.

33. Ramkumar, N.; Omelchenko, T.; Silva-Gagliardi, N.F.; McGlade, C.J.; Wijnholds, J.; Anderson, K.V. Crumbs2 promotes cell ingression during the epithelial-to-mesenchymal transition at gastrulation. *Nat. Cell Biol. 2016 1812* **2016**, *18*, 1281–1291.
34. Ebarasi, L.; Ashraf, S.; Bierzynska, A.; Gee, H.Y.; McCarthy, H.J.; Lovric, S.; Sadowski, C.E.; Pabst, W.; Vega-Warner, V.; Fang, H.; et al. Defects of CRB2 cause steroid-resistant nephrotic syndrome. *Am. J. Hum. Genet.* **2015**, *96*, 153–61.
35. Slavotinek, A.; Kaylor, J.; Pierce, H.; Cahr, M.; DeWard, S.J.; Schneidman-Duhovny, D.; Alsadah, A.; Salem, F.; Schmajuk, G.; Mehta, L. CRB2 mutations produce a phenotype resembling congenital nephrosis, Finnish type, with cerebral ventriculomegaly and raised alpha-fetoprotein. *Am. J. Hum. Genet.* **2015**, *96*, 162–9.
36. Chen, X.; Jiang, C.; Yang, D.; Sun, R.; Wang, M.; Sun, H.; Xu, M.; Zhou, L.; Chen, M.; Xie, P.; et al. CRB2 mutation causes autosomal recessive retinitis pigmentosa. *Exp. Eye Res.* **2018**, *180*, 164–173.
37. Lee, T.C.; Almeida, D.; Claros, N.; Abramson, D.H.; Cobrinik, D. Cell cycle-specific and cell type-specific expression of Rb in the developing human retina. *Investig. Ophthalmol. Vis. Sci.* **2006**, *47*, 5590–5598.
38. Pellissier, L.P.; Alves, C.H.; Quinn, P.M.; Vos, R.M.; Tanimoto, N.; Lundvig, D.M.S.; Dudok, J.J.; Hooibrink, B.; Richard, F.; Beck, S.C.; et al. Targeted ablation of CRB1 and CRB2 in retinal progenitor cells mimics Leber congenital amaurosis. *PLoS Genet* **2013**, *9*, e1003976.
39. Quinn, P.M.; Alves, C.H.; Klooster, J.; Wijnholds, J. CRB2 in immature photoreceptors determines the superior-inferior symmetry of the developing retina to maintain retinal structure and function. *Hum. Mol. Genet.* **2018**, *27*, 3137–3153.
40. Surace, E.M.; Auricchio, A.; Reich, S.J.; Rex, T.; Glover, E.; Pineles, S.; Tang, W.; O'Connor, E.; Lyubarsky, A.; Savchenko, A.; et al. Delivery of Adeno-Associated Virus Vectors to the Fetal Retina: Impact of Viral Capsid Proteins on Retinal Neuronal Progenitor Transduction. *J. Virol.* **2003**, *77*, 7957–7963.
41. Petit, L.; Ma, S.; Cheng, S.-Y.; Gao, G.; Punzo, C. Rod Outer Segment Development Influences AAV-Mediated Photoreceptor Transduction After Subretinal Injection. *Hum. Gene Ther.* **2017**, *28*, 464–481.
42. Fuchs, M.; Brandstätter, J.H.; Regus-Leidig, H. Evidence for a Clathrin-independent mode of endocytosis at a continuously active sensory synapse. *Front. Cell. Neurosci.* **2014**, *8*, 1–13.
43. Vandenberghe, L.H.; Bell, P.; Maguire, A.M.; Cearley, C.N.; Xiao, R.; Calcedo, R.; Wang, L.; Castle, M.J.; Maguire, A.C.; Grant, R.; et al. Dosage thresholds for AAV2 and AAV8 photoreceptor gene therapy in monkey. *Sci. Transl. Med.* **2011**, *3*, 88ra54.
44. Pearson, R.A.; Barber, A.C.; West, E.L.; MacLaren, R.E.; Duran, Y.; Bainbridge, J.W.; Sowden, J.C.; Ali, R.R. Targeted disruption of outer limiting membrane junctional proteins (Crb1 and ZO-1) increases integration of transplanted photoreceptor precursors into the adult wild-type and degenerating retina. *Cell Transplant.* **2010**, *19*, 487–503.
45. Dambrot, C.; Buermans, H.P.J.; Varga, E.; Kosmidis, G.; Langenberg, K.; Casini, S.; Elliott, D.A.; Dinnyes, A.; Atsma, D.E.; Mummery, C.L.; et al. Strategies for rapidly mapping proviral integration sites and assessing cardiogenic potential of nascent human induced pluripotent stem cell clones. *Exp. Cell Res.* **2014**, *327*, 297–306.
46. Chen, X.; Janssen, J.M.; Liu, J.; Maggio, I.; 't Jong, A.E.J.; Mikkers, H.M.M.; Gonçalves, M.A.F. V In trans paired nicking triggers seamless genome editing without double-stranded DNA cutting. *Nat. Commun.* **2017**, *8*, 657.
47. Klooster, J.; Blokker, J.; ten Brink, J.B.; Unmehopa, U.; Fluiter, K.; Bergen, A.A.B.; Kamermans, M. Ultrastructural localization and expression of TRPM1 in the human retina. *Investig. Ophthalmol. Vis. Sci.* **2011**, *52*, 8356–8362.
48. Alves, C.H.; Pellissier, L.P.; Vos, R.M.; Garcia Garrido, M.; Sothilingam, V.; Seide, C.; Beck, S.C.; Klooster, J.; Furukawa, T.; Flannery, J.G.; et al. Targeted ablation of Crb2 in photoreceptor cells induces retinitis pigmentosa. *Hum. Mol. Genet.* **2014**, *23*, 3384–3401.
49. Buck, T.M.; Pellissier, L.P.; Vos, R.M.; van Dijk, E.H.C.C.; Boon, C.J.F.; Wijnholds, J. AAV serotype testing on cultured human donor retinal explants. In *Methods in Molecular Biology*; Boon, C.J.F., Wijnholds, J., Eds.; New York, NY: Humana Press: New York, NY, 2018; Vol. 1715, p. pp 275-288 ISBN 978-1-4939-7522-8.

FIGURES

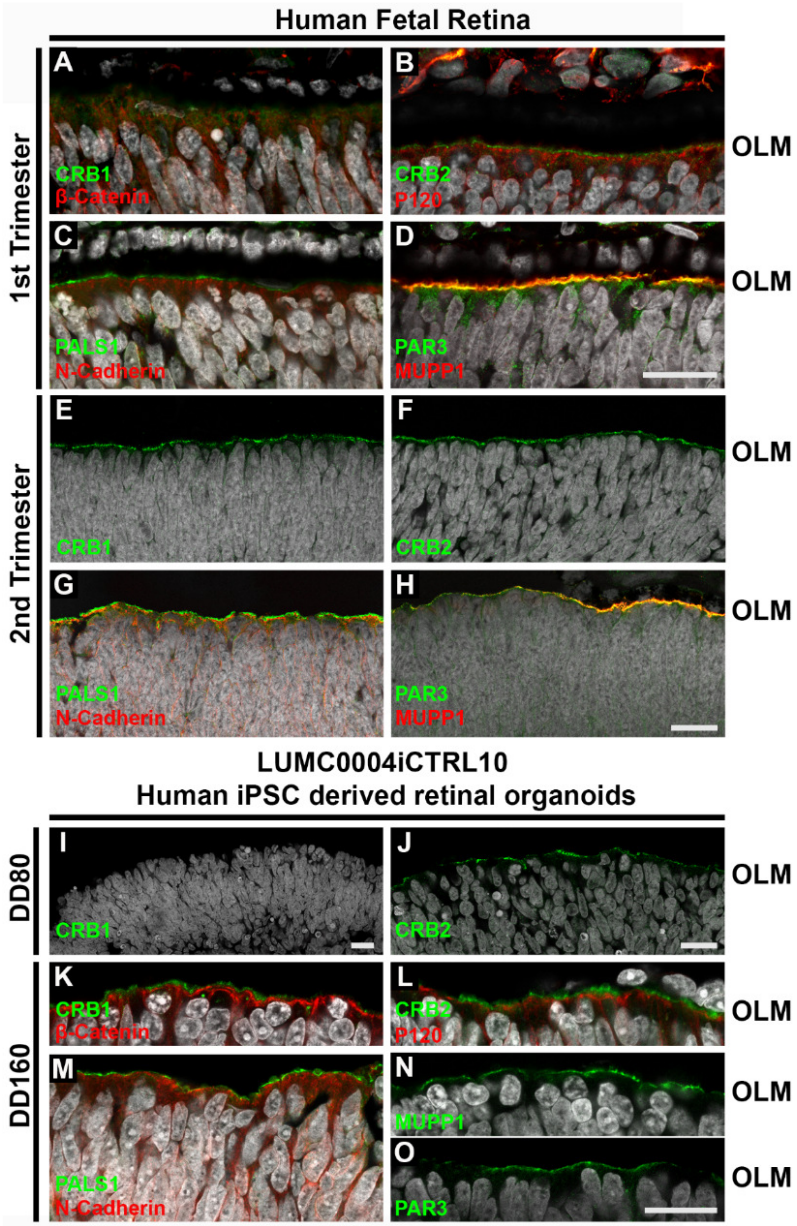

Figure 1. Localization of the CRB complex at the outer limiting membrane in human fetal and iPSC-derived human retina. Immunohistochemistry pictures of 1st (A-D) and 2nd (E-H) trimester human fetal retina and early (I, J) and late (K-O) LUMC0004iCTRL10 hiPSC-derived retinal organoids. Sections were stained for subapical region markers: CRB1 (A, E, I, K), CRB2 (B, F, J, L) PALS1 (C, G, M), PAR3 (D, H, O), MUPP1 (D, H, N) and for adherens junction markers: β-catenin (A, K), p120-catenin (B, L), N-cadherin (C, G, M). OLM, outer limiting membrane. Scale bars: (A-0), 20μm. See also Figure S1 and S2.

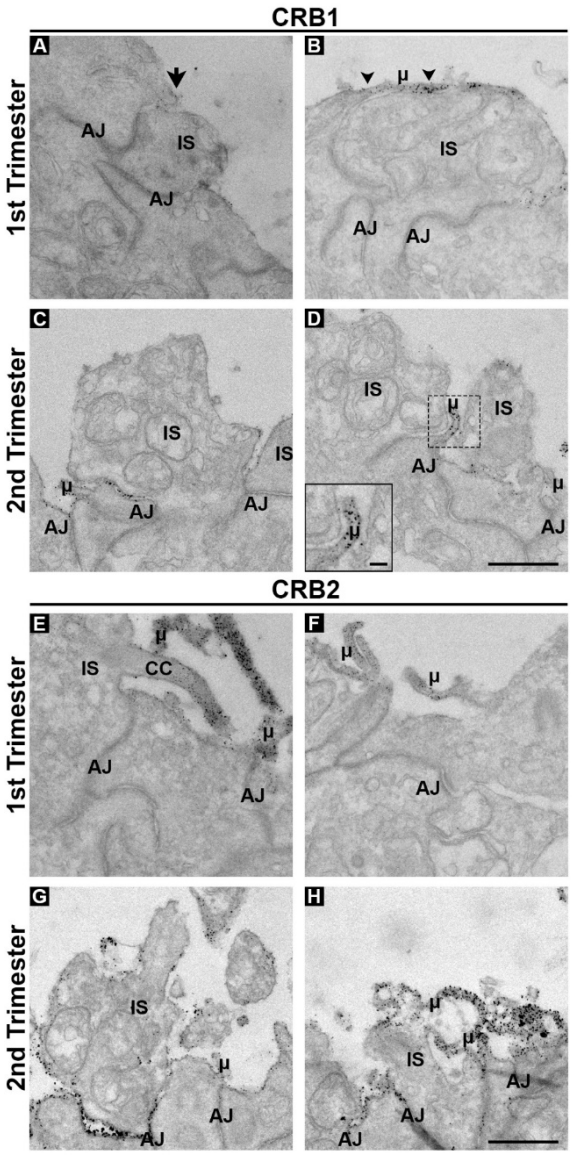

Figure 2. CRB1 and CRB2 are located at the outer limiting membrane in Müller glial cells and photoreceptors of 1st and 2nd Trimester human fetal retina. Immuno-EM staining showing the localisation of CRB1 (A-D) and CRB2 (E-H) in 1st (A, B, E, F) and 2nd (C, D, G, H) trimester human fetal retina. CRB1 was sporadically detected in the 1st trimester but being found subapically of adherens junctions adjacent to photoreceptor inner segments (A, arrow) and in Müller glial cell apical villi (B, arrowheads). In the 2nd trimester, CRB1 was found consistently throughout the outer limiting membrane of human fetal retina subapically of adherens junctions of photoreceptors and Müller glial cells (C, D). CRB2 was localised in both 1st and 2nd trimester retina subapically of adherens junctions being located in photoreceptor inner segments and apical villi of Müller glial cells. At least two independent samples were analysed per time point. CC, connecting cilium; AJ, adherens junction; μ, microvilli; IS, inner segment. Scale bar: 1μm, inserts: 500nm.

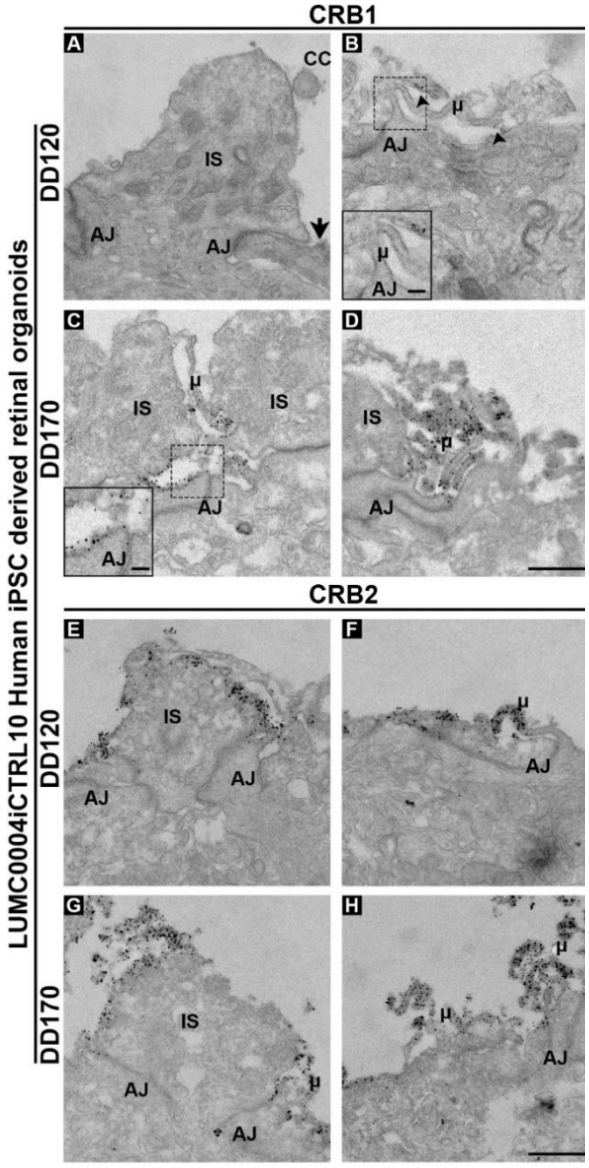

Figure 3. CRB1 and CRB2 are located at the outer limiting membrane in Müller glial cells and photoreceptors of human iPSC-derived retinal organoids. Immuno-EM staining showing the localisation of CRB1 (A-D) and CRB2 (E-H) in DD120 (A, B, E, F) and DD170 (C, D, G, H) LUMC0004iCTRL10 human iPSC-derived retinal organoids. CRB1 was lowly and sporadically detected at DD120 but being found subapically of adherens junctions adjacent to photoreceptor inner segments (A, arrow) and in Müller glial cell apical villi (B, arrowheads). At DD170 CRB1 was found consistently throughout the outer limiting membrane of human iPSC-derived retinal organoids subapically of adherens junctions of photoreceptors and Müller glial cells (C, D). CRB2 was localised at both DD120 and DD170 subapically of adherens junctions being located in photoreceptor inner segments and apical villi of Müller glial cells. At least two independent samples were analysed per time point. CC, connecting cilium; AJ, adherens junction; μ, microvilli; IS, inner segment. Scale bar: 1μm, inserts: 500nm.

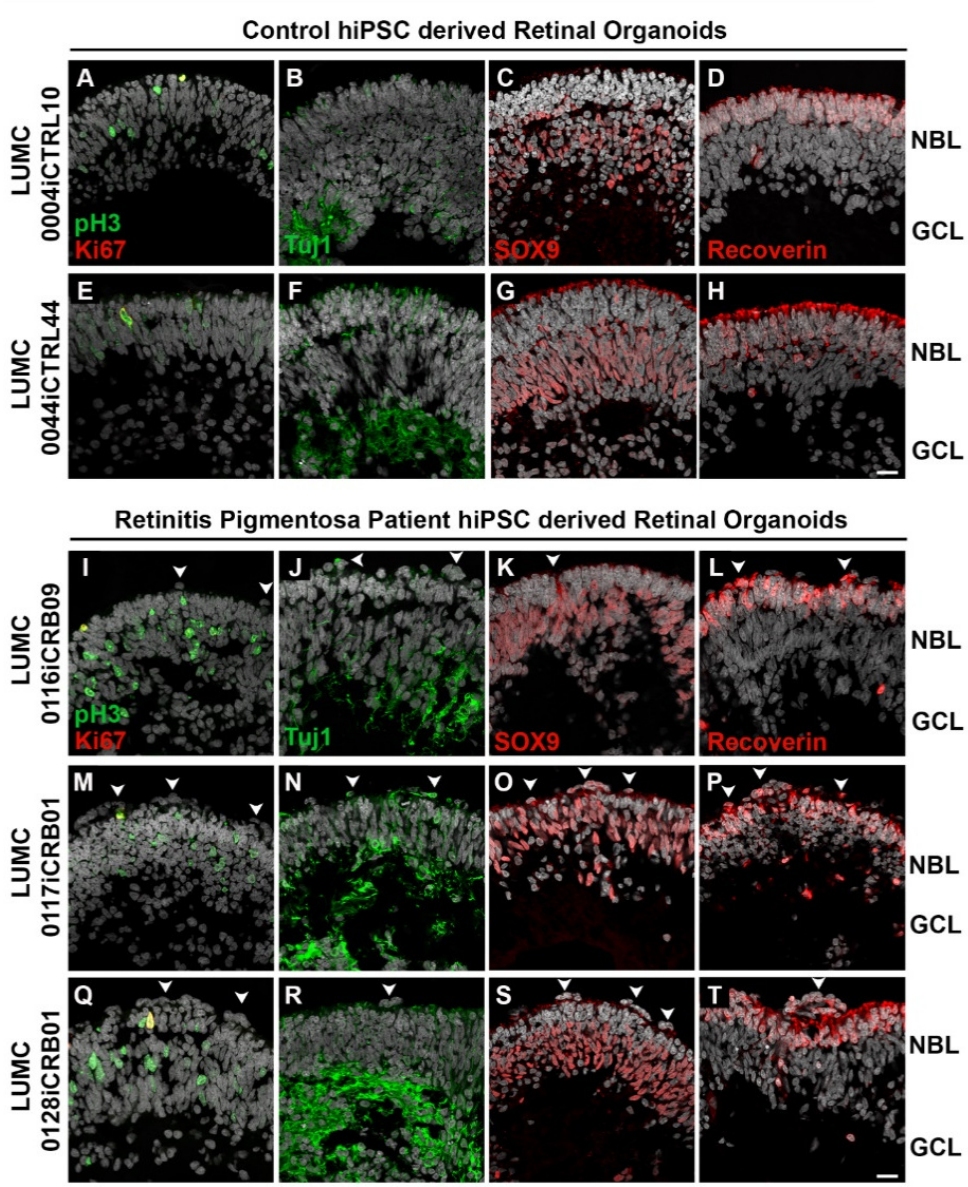

Figure 4. *CRB1* patient retinal organoids develop proper lamination. Immunohistochemistry pictures of healthy (LUMC0004iCTRL10; LUMC0044iCTRL44) vs *CRB1* patient (LUMC0116iCRB09, LUMC0117iCRB01, LUMC0128iCRB01) retinal organoids at DD180. Sections were stained for pH3^{+} mitotic cells and Ki67^{+} cycling cells (A, E, I, M, Q); Tuj1^{+} dendrites marking the GCL (B, F, J, N, R); SOX9^{+} NBL cells (C, G, K, O, S); and recoverin^{+} PRCs marking the ONL (D, H, L, P, T). Experiments were validated in two differentiations for retinal organoids. NBL, neurobasal layer; GCL, ganglion cell layer. Scale bars: (A-0), 20µm. See also Figure S4.

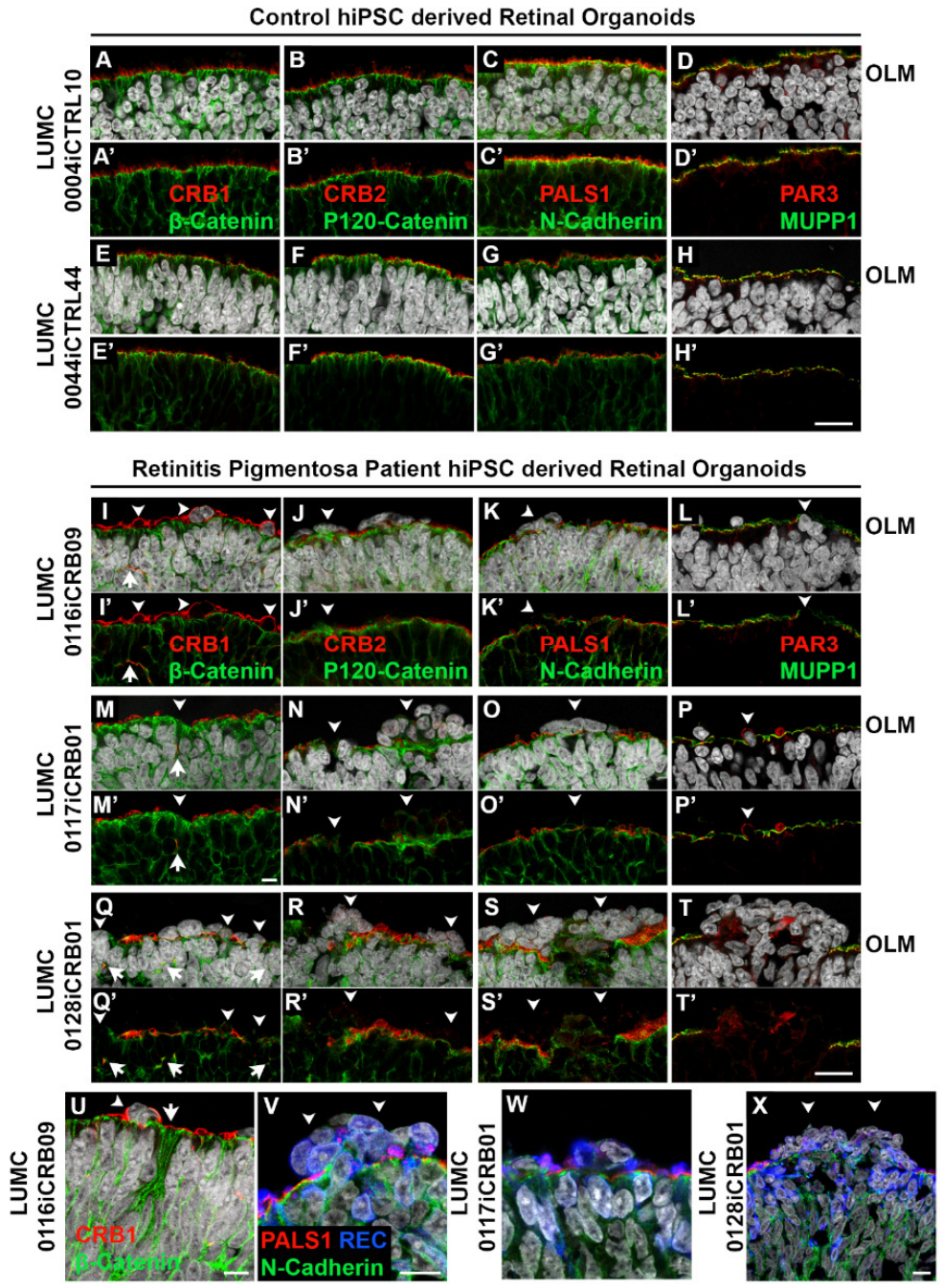
Control hiPSC derived Retinal Organoids
LUMC 0004iCTRL10
LUMC 0044iCTRL44
OLM
CRB1
β-Catenin
CRB2
P120-Catenin
PALS1
N-Cadherin
PAR3
MUPP1
Retinitis Pigmentosa Patient hiPSC derived Retinal Organoids
LUMC 0116iCRB09
LUMC 0117iCRB01
LUMC 0128iCRB01
PALS1 REC
N-Cadherin

Figure 5. *CRB1* patient organoids develop retinal degeneration. Immunohistochemistry pictures of healthy (LUMC0004iCTRL10 (A-D, A'-D'); LUMC0044iCTRL44 (E-H, E'-H')) and *CRB1* patient (LUMC0116iCRB09 (I-L, I'-L', U, V), LUMC0117iCRB01 (M-P, M'-P', W), LUMC0128iCRB01 (Q-T, Q'-T, X)) retinal organoids at DD180. Sections were stained for subapical region markers: CRB1 (A, E, I, M, Q, U), CRB2 (B, F, J, N, R), PALS1 (C, G, K, O, S, V, W, X), PAR3 (D, H, L, P,T), MUPP1 (D, H, L,P,T) and for adherens junction markers: β-catenin (A, E, I, M, Q, U), p120-catenin (B,F,J,N,R), N-cadherin (C,G,K,O,S,V). Disruptions of the OLM are seen in patient retinal organoids (I-T, I'-T') with recoverin^{+} photoreceptors found displaced (V-X). A-X counterstained with DAPI. Experiments were validated in two differentiations for retinal organoids. OLM, outer limiting membrane; NBL, neurobasal layer. Scale bars: (A-0), 20μm. See also Figure S4.

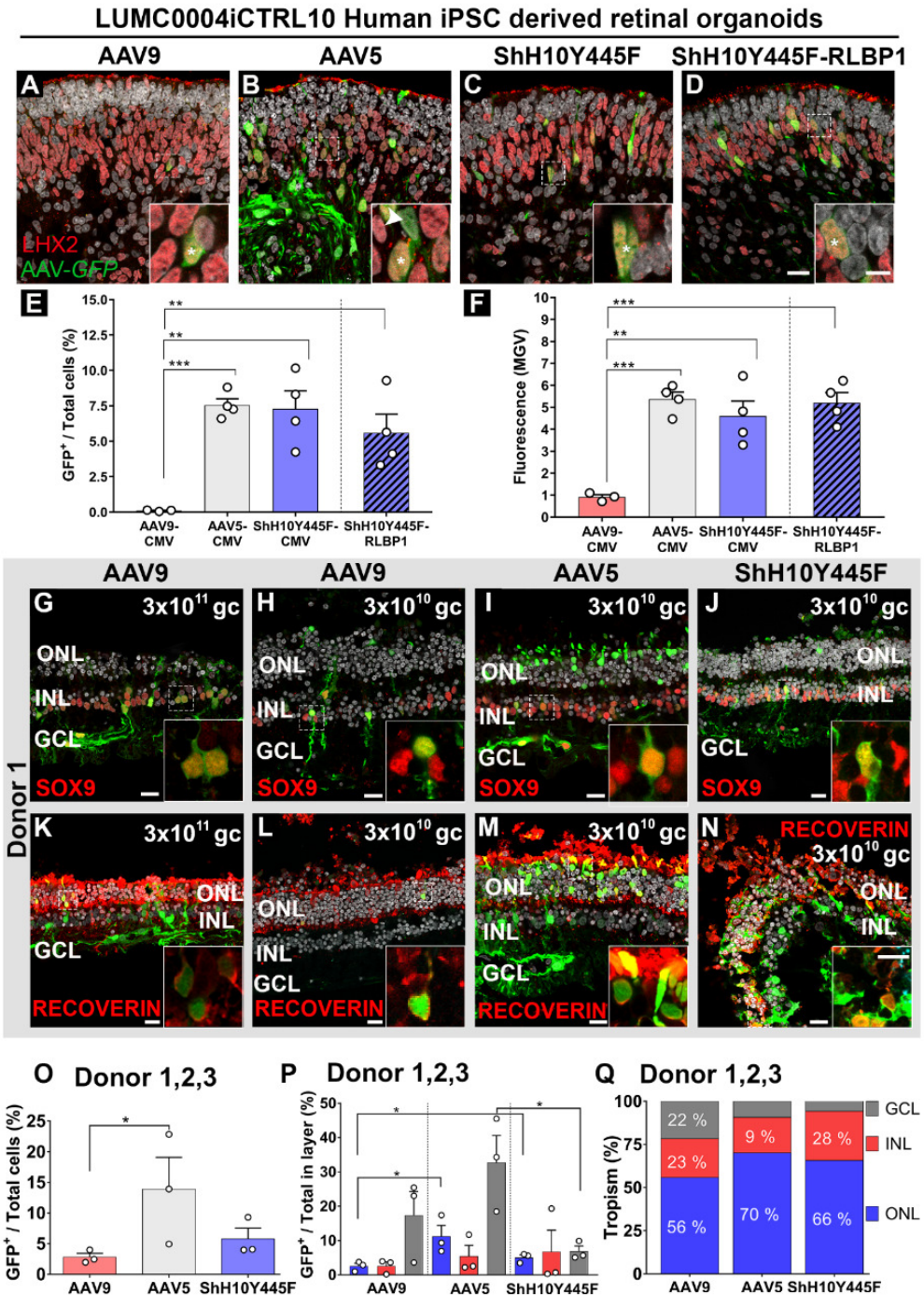
LUMC0004iCTRL10 Human iPSC derived retinal organoids
AAV9
AAV5
ShH10Y445F
ShH10Y445F-RLBP1
A
B
C
D
LHX2
AAV-GFP
E
GFP+ / Total cells (%)
AAV9-CMV
AAV5-CMV
ShH10Y445F-CMV
ShH10Y445F-RLBP1
F
Fluorescence (MGV)
Donor 1
G 3x10^11 gc
H 3x10^10 gc
I 3x10^10 gc
J 3x10^10 gc
ONL
INL
GCL
SOX9
K 3x10^11 gc
L 3x10^10 gc
M 3x10^10 gc
N RECOVERIN 3x10^10 gc
RECOVERIN
O Donor 1,2,3
GFP+ / Total cells (%)
P Donor 1,2,3
GFP+ / Total in layer (%)
Q Donor 1,2,3
Tropism (%)
22 %
23 %
56 %
9 %
70 %
28 %
66 %
GCL
INL
ONL

Figure 6. AAV5 and ShH10Y445F efficiently infect Müller glial cells in human iPSC retinal organoids and photoreceptors and Müller glial cells in the human adult retina. Infection of 7.5-month-old LUMC0004iCTRL10 hiPSC retinal organoids at 10^{10} gc with AAV9-CMV-*GFP* (A), AAV5-CMV-*GFP* (B), ShH10Y445F-CMV-*GFP* (C) and ShH10Y445F-RLBP1-*GFP* (D) and co-staining with the Müller glial cell marker LHX2, the majority of LHX2$^+$ cells were also GFP$^+$ (asterisk). Efficacy of transducing retinal cell types was quantified by measuring the number of GFP$^+$ cells in the total cell population (E) and fluorescence (MGV) (F). AAV5 and ShH10Y445F showed the higher efficacy of transducing retinal cell types at 10^{10} gc than AAV9, which showed lower efficacy. 10^{10} gc applied per 2 organoids, two independent differentiations used, 3-4 organoids analysed per vector. Infection of human retinal explants with AAV9-CMV-*GFP* at $3x10^{11}$ gc (G, K) and $3x10^{10}$ gc (H, L), AAV5-CMV-*GFP* at $3x10^{10}$ gc (I, M) and ShH10Y445F-CMV-*GFP* at $3x10^{10}$ gc (J, N). Co-staining showed the presence of GFP$^+$ /Sox9$^+$ Müller glial cells with AAV9 (G, H), AAV5 (I), and ShH10Y445F (J). Co-staining showed the presence of GFP$^+$ /recoverin$^+$ photoreceptors AAV9 (K, L), AAV5 (M), and ShH10Y445F (N). Efficacy of transducing retinal cell types at $3x10^{10}$ gc was quantified by measuring the number of GFP$^+$ cells in the total cell population (O). When compared for 3 donors at $3x10^{10}$ gc, AAV5 showed higher efficacy of transducing retinal cell types than AAV9. The potency of AAV serotypes was compared by analysing transduction of cell types in each of the ONL, INL and GCL (P). AAV5 and ShH10Y445F showed higher potency in transduction of photoreceptors in the ONL than AAV9. All serotypes transduced cells in all layers at $3x10^{10}$ gc (Q). Each dot represents the average of an individual donor (O, P), 10 images were analysed per donor (O-Q) ONL, outer nuclear layer; INL, inner nuclear layer; GCL, ganglion cell layer; gc, genome copies; MGV, mean grey value. Scale bar: (A-N), 20µm; (G-N) inserts 10µm. Data are presented as mean ± SEM. $*p < 0.05$. See also Figure S5, S6 and S7.

Supplementary Figures and Legends

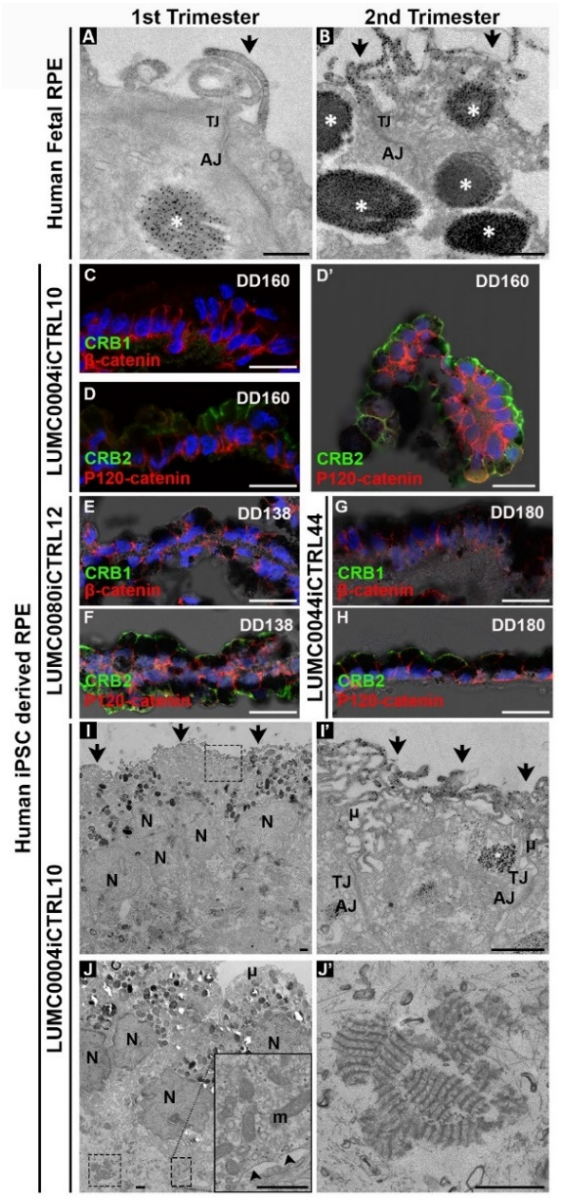

Figure 7. Human iPSC retinal pigment epithelium localise CRB2 at and above tight junctions in the apical membrane and microvilli. Immuno-EM showed staining for CRB2 above adherens junctions at and above tight junctions in the apical membrane and in the microvilli in 1st (A) and 2nd (B) trimester in human fetal RPE. Aspecific staining was detected within melanosomes (A and B, asterisk). Immunohistochemistry did not detect CRB1 apically of β-catenin (C) in hiPSC RPE, but CRB2 was found apically of p120-catenin in LUMC0004iCTRL10 (D, D'), LUMC0080iCTRL12 (E, F) and LUMC0044iCTRL44 (G, H) human iPSC-derived RPE. RPE spheroids were found either attached to retinal organoids or became independent, detached spheroids (D'). Immuno-EM confirmed apical staining for CRB2 above adherens junctions at and above tight junctions in the apical membrane and in the microvilli (I and I', arrows). Aspecific staining was detected within pigmented melanosomes (I', asterisk). Electron microscopy of hiPSC-derived RPE also showed basally located mitochondria (J, insert) and basement membrane (J, insert arrowheads) and fibrous long-spacing collagen (FLSC) (J and J'). AJ, adherens junction; N, nuclei; μ, microvilli; TJ, tight junction; m, mitochondria. Scale bars: (A, B, B', E, F, G, H) 20μm, (C, C', D, D', insert D) 1μm.

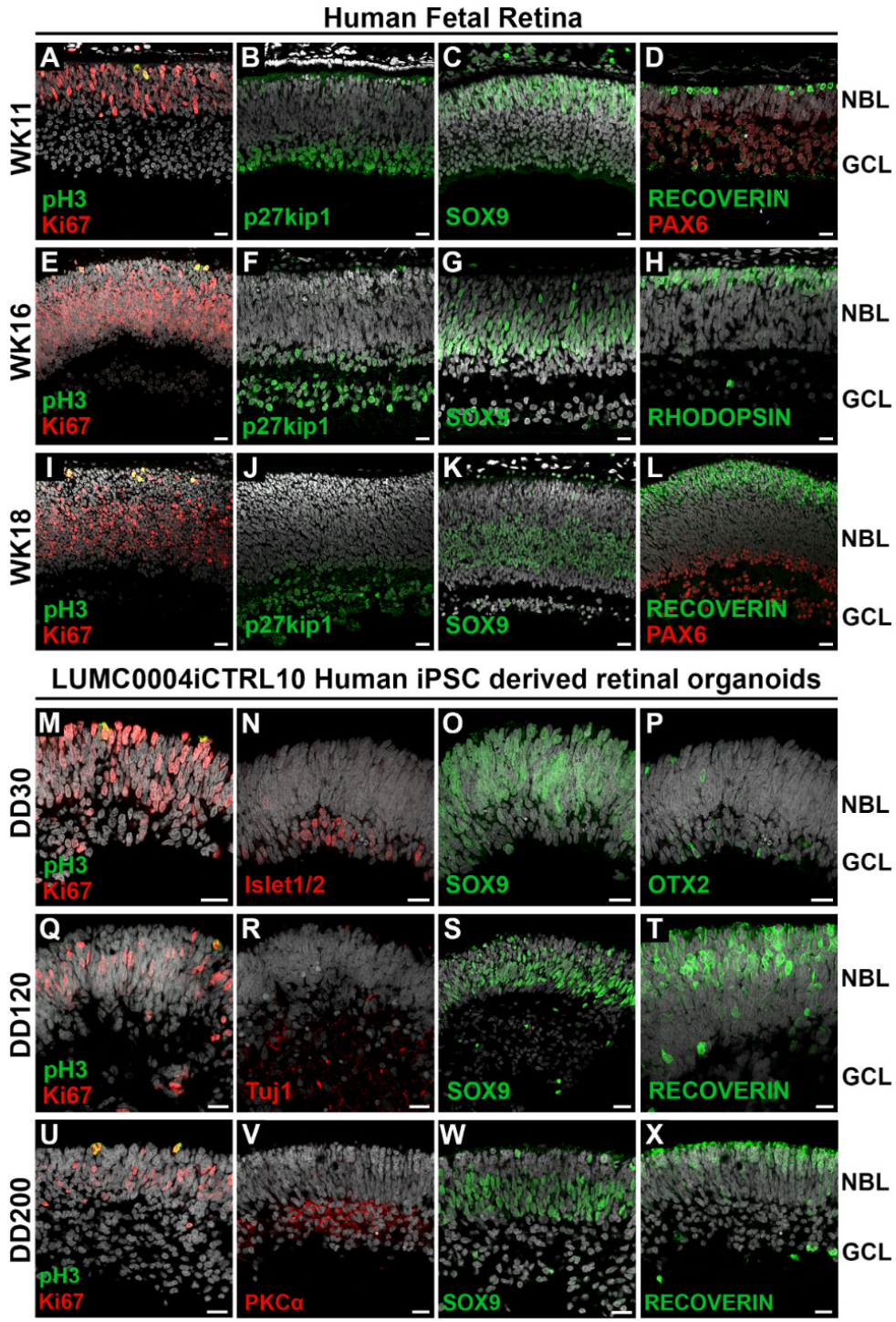
Human Fetal Retina
WK11
WK16
WK18
A
B
C
D
E
F
G
H
I
J
K
L
pH3
Ki67
p27kip1
SOX9
RECOVERIN
PAX6
RHODOPSIN
NBL
GCL
LUMC0004iCTRL10 Human iPSC derived retinal organoids
DD30
DD120
DD200
M
N
O
P
Q
R
S
T
U
V
W
X
Islet1/2
OTX2
Tuj1
PKCα

Figure S1. Retinal architecture in the human fetal retina and human iPSC retinal organoids. Related to Figure 1. Immunohistochemistry pictures of WK11 (A-D), WK16 (E-H) and WK18 (I-L) human fetal retina and DD30 (M-P), DD120 (Q-T) and D200 (U-X) LUMC0004iCTRL10 hiPSC-derived retinal organoids. Sections were stained with antibodies against: Ki67 (A, E, I, M, Q, U), pH3 (A, E, I, M, Q, U), $p27^{kip1}$ (B, F, J), SOX9 (C, G, K, O, S, W), Recoverin (D, L, T, X), PAX6 (D, L), Rhodopsin (H), Islet1/2 (N), Tuj1 (R), PKCα (V), OTX2 (P). In human fetal retina at week 11 in the 1st trimester of pregnancy we observed cycling cells that stained positive for anti-Ki67 and spanned the thickness of the neuroblast layer (NBL). The mitotic cells located most apically and stained positive for pH3 (A). Inner retinal cells as marked by p27kip1 and PAX6 were restricted to the ganglion cell layer and a subset of cells in the NBL (B and D). The cells that exited the cell cycle were marked with p27kip1, whereas the ganglion cells, amacrine cells and migrating retinal progenitors were marked with PAX6. Radial glial progenitor cell nuclei spanned the thickness of the NBL and stained positive for anti-SOX9 (C). Newborn cone photoreceptors marked positive for anti-recoverin (D (See also Figure S2A and S2B)). In the human fetal retina at weeks 16 and 18 in the 2nd trimester of pregnancy, we observed the localisation of anti-pH3-positive mitotic cells most apically within the NBL (E and I). However, the cycling anti-Ki67-positive cells became mostly restricted to the middle NBL cells but also labelled occasional outer NBL cells (E and I). Both p27kip1- and PAX6-positive cells restricted to the inner NBL and the ganglion cell layer (F, J, L). SOX9-positive cell nuclei localised in the middle NBL and occasionally the outer NBL, marking at this stage of development both the maturing Müller glial cells and radial glial progenitor cells (G (See also Figure S2C)). The outer NBL showed an increase in recoverin-positive photoreceptors at weeks 16 and 18 compared to week 11 (H and L). Rhodopsin-positive staining indicated the presence of rod photoreceptors whose basal processes extended from the outer NBL to the bottom of the inner NBL (H). In early DD30 hiPSC retinal organoids we observed that Ki67-positive cycling cells spanned the thickness of the NBL with pH3-positive mitotic cells located most apically (M). Ki67-positive cycling cells were also detected in the ganglion cell layer (GCL). Islet1/2-positive cells were found mostly restricted to the GCL with sporadic cells in the NBL (Figure 1N). SOX9-positive radial glial progenitor cell nuclei spanned the thickness of the NBL but were also seen occasionally in the GCL (Figure 1O). Immature photoreceptors that stained positive for anti-OTX2 could be found in both the NBL and GCL (Figure 1P). In later DD120 and DD200 hiPSC-derived retinal organoids Ki67-positive cycling cells restricted mostly to the middle NBL but occasionally were detected in the outer NBL and in the GCL, whereas pH3-positive mitotic cells located apically (Q and U). In the inner retina Tuj1-positive ganglion cell axons (R) and PKCα-positive bipolar cells (V) were detected. SOX9-positive cell nuclei became more restricted to the middle NBL but occasionally were detected in the outer NBL and the GCL (S and W (See also Figure S2D)). Recoverin-positive photoreceptor cells were mostly restricted to the outer NBL. Some recoverin-positive cells were detected within the NBL and occasional recoverin-positive cells were detected in the GCL (T and X). At least two independent differentiations/samples were analysed, 3-6 sections examined per organoid or fetal eye. Scale bars: (A-X), 20μm.

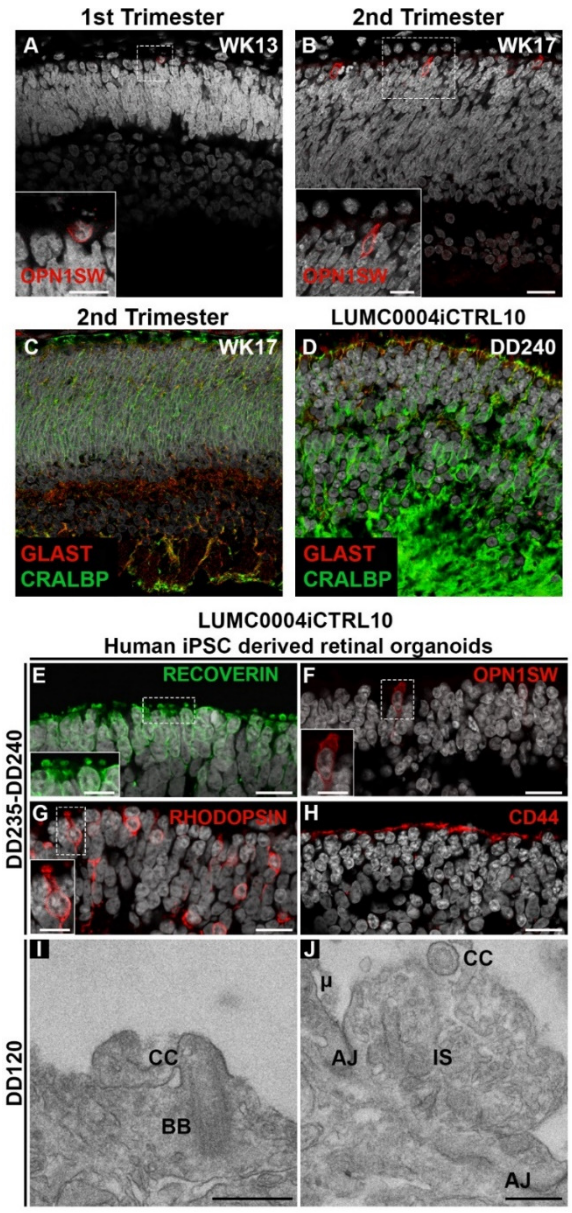

Figure S2. Long-term maturation of fetal retinas and human iPSC retinal organoids. Related to Figures 1 and S1. Immunohistochemistry pictures of 1st and 2nd trimester fetal retina (A-C) and LUMC0004iCTRL10 human iPSC-derived retinal organoids (D-J). Sections were stained for OPN1SW (A, B, F), RLBP1 and GLAST (C, D), Recoverin (E), Rhodopsin (G), and CD44 (H). Human fetal retina had cones in the 1st (A) and 2nd trimester (B) and Müller glial cells in the 2nd trimester (D). Immature photoreceptor segments were detected in human iPSC retinal organoid (E) with the presence of both cones (F) and rods (G). Additionally, staining of CRALBP, GLAST and CD44 suggested the presence of Müller glial cells (D, H). Electron microscopy at DD120 confirmed a number of retinal structures including: basal bodies (I), connecting cilium (I,J), inner segment (J), adherens junction (J), microvilli (J). At least two independent differentiations/samples were analysed, 3-6 sections examined per organoid or fetal eye. CC =connecting cilium; IS = inner segment; BB =basal body; AJ adherens junction; μ= microvilli. Scale bars: (A-H), 20μm; inserts (A, B, E, F, G) 10 μm, (I, J) 500nm.

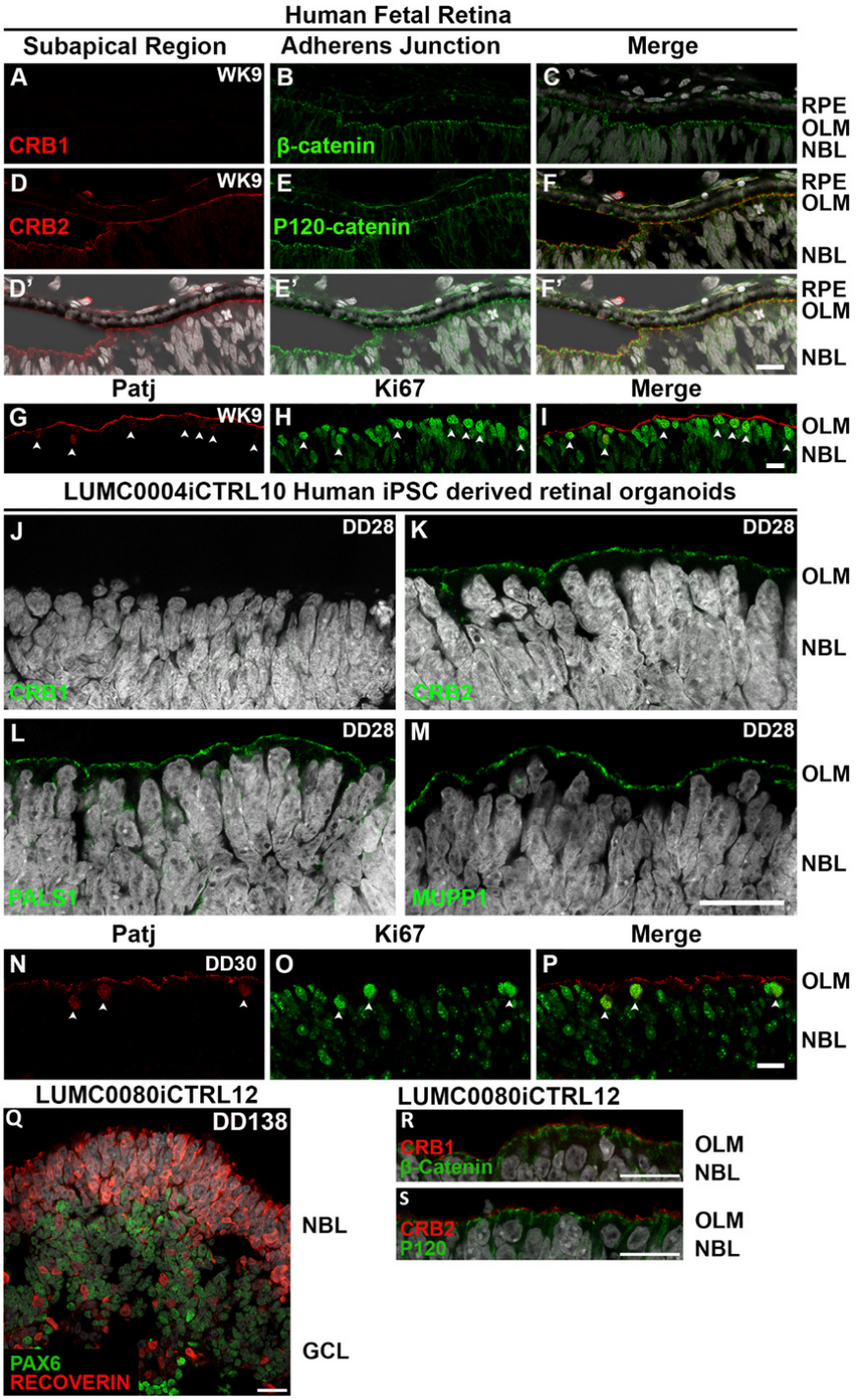
Human Fetal Retina
Subapical Region
Adherens Junction
Merge
A
WK9
CRB1
B
β-catenin
C
RPE
OLM
NBL
D
WK9
CRB2
E
P120-catenin
F
RPE
OLM
NBL
D'
E'
F'
RPE
OLM
NBL
Patj
Ki67
Merge
G
WK9
H
I
OLM
NBL
LUMC0004iCTRL10 Human iPSC derived retinal organoids
J
DD28
CRB1
K
DD28
CRB2
OLM
NBL
L
DD28
PALS1
M
DD28
MUPP1
OLM
NBL
Patj
Ki67
Merge
N
DD30
O
P
OLM
NBL
LUMC0080iCTRL12
Q
DD138
PAX6
RECOVERIN
NBL
GCL
LUMC0080iCTRL12
R
CRB1
β-Catenin
OLM
NBL
S
CRB2
P120
OLM
NBL

Figure S3. Localisation of CRB complex in the 1st trimester fetal retina and early and late human iPSC retinal organoids. Related to Figure 1, 4 and 5. Immunohistochemistry pictures of week 9 1st Trimester human fetal retina (A-I), DD28 LUMC0004iCTRL10 human iPSC-derived retinal organoids (J-P) and retinal organoids derived from hiPSC lines LUMC0080iCTRL12 (Q, R, S). Sections were stained with antibodies against: CRB1 and β-catenin (A-C), CRB2 and p120-catenin (D-F, D'-F'), PATJ and Ki67 (G-I) in week 9 human fetal retina. Sections were stained with antibodies against: CRB1 (J), CRB2 (K), PALS1 (L), MUPP1 (M), PATJ and Ki67 (N-P) in DD28-30 human iPSC-derived retinal organoids. Sections were stained with antibodies against: Recoverin and PAX6 (Q), CRB1 and β-catenin (R), CRB2 and p120-catenin (S) from retinal organoids derived from hiPSC lines LUMC0080iCTRL12. CRB1 was not found subapically of β-catenin (A-C) but CRB2 was found subapically of p120-catenin (D-F, D'-F') in week 9 human fetal retina. CRB2 was detected in week 9 fetal retinal pigment epithelium (D'-F'). PATJ was observed at the outer limiting membrane and also co-stained a subset of Ki67-positive cells (G-I, arrowheads) in week 9 human fetal retina. In DD28 human iPSC-derived retinal organoids CRB1 was not found at the subapical region (J) but CRB2 (K), PALS1 (L) and MUPP1 (M) were. PATJ also co-stained a subset of Ki67-positive cells in DD28 human iPSC-derived retinal organoids (N-P, arrowheads). Human iPSC lines LUMC0080iCTRL12 formed retinal organoids (Q). CRB1 was found subapically of β-catenin (R) and CRB2 was found subapically of p120-catenin (S). At least two independent differentiations/samples were analysed, 3-6 sections examined per organoid or fetal eye. RPE, retinal pigment epithelium; OLM, outer limitting membrane; NBL, neuroblast layer. Scale bars: 20μm (A-S).

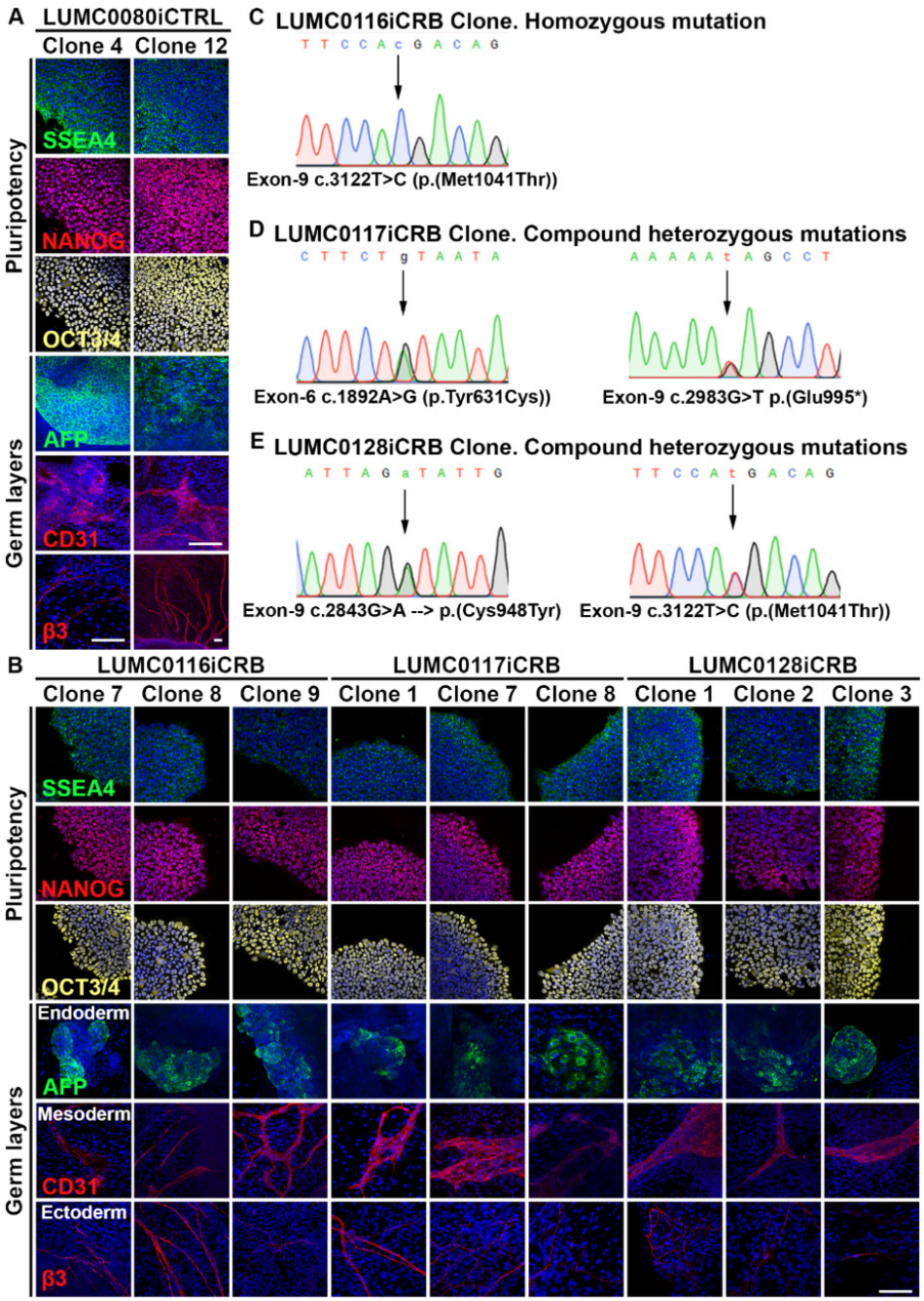
A
LUMC0080iCTRL
Clone 4
Clone 12
Pluripotency
SSEA4
NANOG
OCT3/4
Germ layers
AFP
CD31
β3
C
LUMC0116iCRB Clone. Homozygous mutation
Exon-9 c.3122T>C (p.(Met1041Thr))
D
LUMC0117iCRB Clone. Compound heterozygous mutations
Exon-6 c.1892A>G (p.Tyr631Cys))
Exon-9 c.2983G>T p.(Glu995*)
E
LUMC0128iCRB Clone. Compound heterozygous mutations
Exon-9 c.2843G>A --> p.(Cys948Tyr)
Exon-9 c.3122T>C (p.(Met1041Thr))
B
LUMC0116iCRB
LUMC0117iCRB
LUMC0128iCRB
Clone 7
Clone 8
Clone 9
Clone 1
Clone 7
Clone 8
Clone 1
Clone 2
Clone 3
Pluripotency
SSEA4
NANOG
OCT3/4
Germ layers
Endoderm
AFP
Mesoderm
CD31
Ectoderm
β3

Figure S4. Generation of human iPSC lines of *CRB1*-related retinitis pigmentosa patients. Related to Figures 4 and 5. Immunohistochemistry pictures of the characterization and validation of human iPSCs for pluripotency (SSEA4, NANOG, OCT3/4) and germ layers (AFP, CD31, β3). LUMC0080iCTRL clones 4 and 12 (A); LUMC0080iCTRL clones 4 and 12 (A); LUMC0116iCRB clones 7, 8, 9 (B); LUMC0117iCRB clones 1, 7, 8 (B); LUMC0128iCRB clones 1, 2, 3 (B). *CRB1* gene exon 6 and 9 was forward and reverse Sanger sequenced for patient lines (LUMC0116iCRB09, C; LUMC0117iCRB01, D; LUMC0128iCRB01, E) and healthy line LUMC0004iCTRL10 (not shown). The mutation in LUMC0116iCRB09 was validated as c.3122T>C (Effect: p(Met1041Thr)) (C). The mutations in LUMC0117iCRB01 was validated as heterozygous mutations with allele 1 being c.1892A>G (Effect: p.Tyr631Cys) and allele 2 being c.2983G>T (Effect: p.(Glu995*) (D). The mutations in LUMC0128iCRB01 was validated as heterozygous mutations with allele 1 being c.2843G>A (Effect: p.(Cys948Tyr) and allele 2 being c.3122T>C (Effect: p(Met1041Thr)) (E). All Scale Bars: 20 µm.

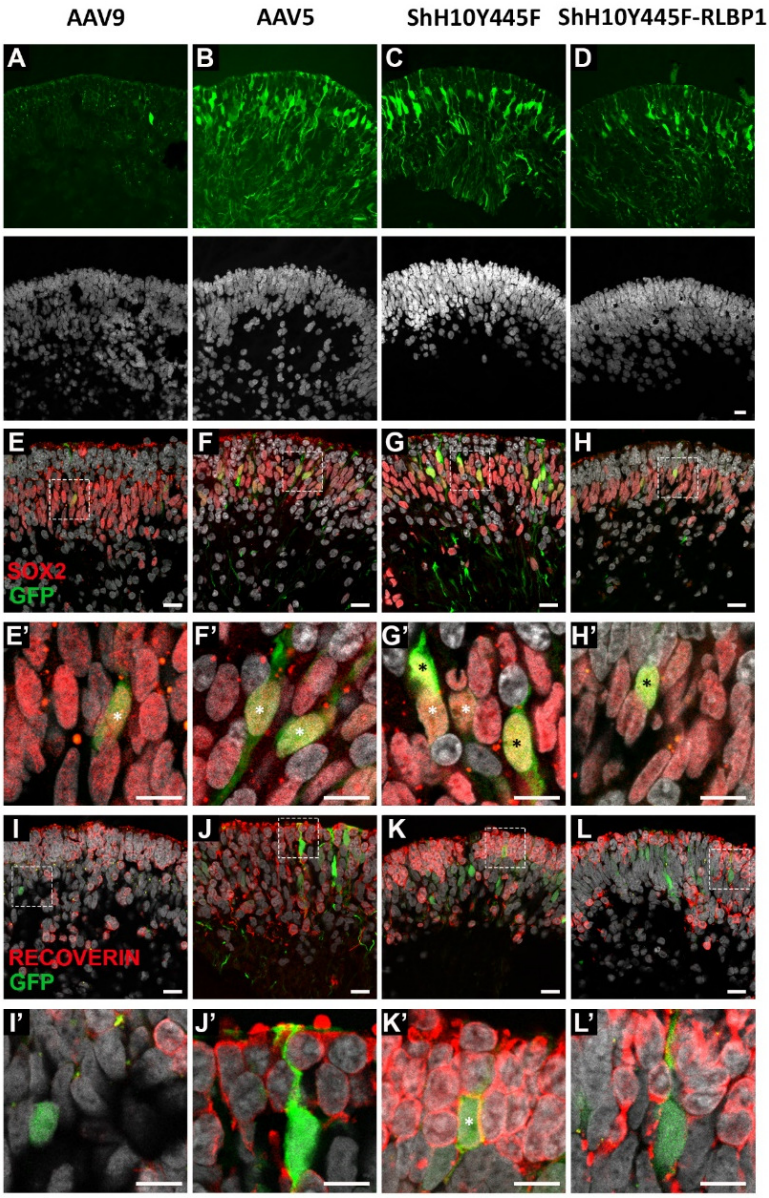

Figure S5. AAV9, AAV5 and ShH10Y445F infect Müller glial cells. Related to Figure 5. Infection of 7.5-month-old LUMC0004iCTRL10 human iPSC-derived retinal organoids at 10^{10}gc with AAV9-CMV-*GFP* (A, E, E', I, I'), AAV5-CMV-*GFP* (B, F, F', J, J'), ShH10Y445F-CMV-*GFP* (C, G, G', K, K') and ShH10Y445F-RLBP1-*GFP* (D, H, H', L, L'). High laser intensity images of AAV9- (A), AAV5- (B), ShH10Y445F-CMV-*GFP* (C) and ShH10Y445F-RLBP1-*GFP* (D). Infection with AAV9- CMV-*GFP*, AAV5- CMV-*GFP*, ShH10Y445F-CMV-*GFP* and ShH10Y445F-RLBP1-*GFP* showed co-staining with Müller glial marker SOX2 (E, F, G, H and inserts E', F', G', H') but not with photoreceptor marker Recoverin (I, J, K, L and inserts I', J', L'). Occasional GFP/recoverin-positive cells were detected (K'). Two independent differentiations of the hiPSC line LUMC0004iCTRL10 were used, 3-6 sections examined per organoid. Scale Bars: 20 µm (A-L), inserts 10 µm (E'-L').

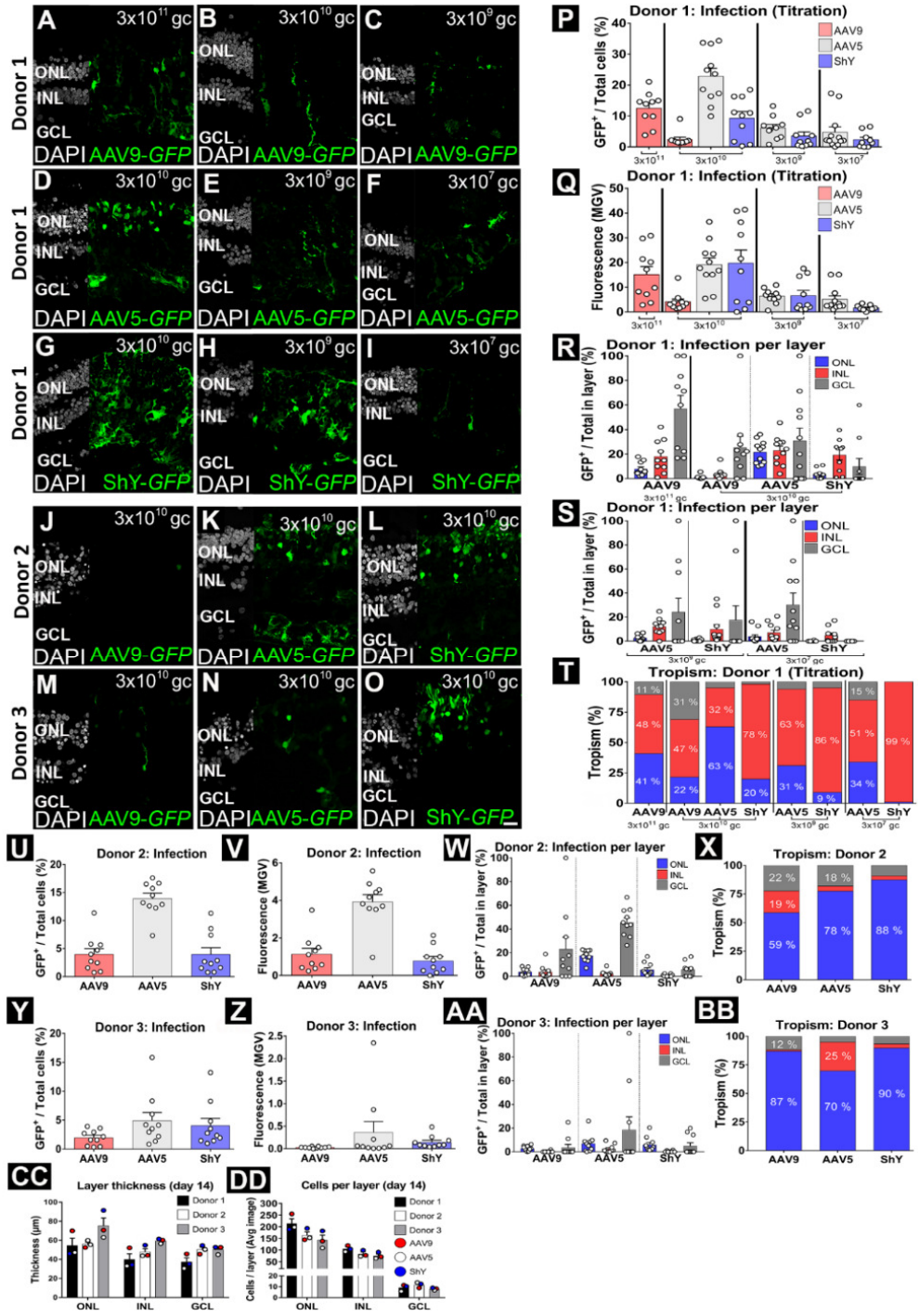
A
3x10^11 gc
B
3x10^10 gc
C
3x10^9 gc
Donor 1
ONL
INL
GCL
DAPI AAV9-GFP
D
3x10^10 gc
E
3x10^9 gc
F
3x10^7 gc
DAPI AAV5-GFP
G
3x10^10 gc
H
3x10^9 gc
I
3x10^7 gc
DAPI ShY-GFP
Donor 2
J
3x10^10 gc
K
3x10^10 gc
L
3x10^10 gc
Donor 3
M
3x10^10 gc
N
3x10^10 gc
O
3x10^10 gc
P
Donor 1: Infection (Titration)
GFP+ / Total cells (%)
AAV9
AAV5
ShY
Q
Donor 1: Infection (Titration)
Fluorescence (MGV)
R
Donor 1: Infection per layer
GFP+ / Total in layer (%)
S
Donor 1: Infection per layer
T
Tropism: Donor 1 (Titration)
Tropism (%)
U
Donor 2: Infection
V
Donor 2: Infection
W
Donor 2: Infection per layer
X
Tropism: Donor 2
Y
Donor 3: Infection
Z
Donor 3: Infection
AA
Donor 3: Infection per layer
BB
Tropism: Donor 3
CC
Layer thickness (day 14)
Thickness (µm)
DD
Cells per layer (day 14)
Cells / layer (Avg image)

Figure S6. Titration of AAV serotypes on human donor 1 retina and independent repeats on donor 2 and 3. Related to Figure 6. Transduction of AAV9- (A-C, J, M), AAV5- (D-F, K, N) and ShH10Y445F (G-I, L, O) on human adult donor retina at $3x10^{11}$ gc (A), $3x10^{10}$ gc (B, D, G, J-O), $3x10^{9}$ gc (C, E, H), $3x10^{7}$ gc (F, I). AAV infection by total GFP-positive cells / Total cells infected for donor 1 (P). Infection measured by GFP-fluorescence for donor 1 (Q). GFP-positive cells per total cells in layer for donor 1 (R, S). Tropism: GFP-positive cells in layer per Total GFP-positive cells for donor 1 (T). Human adult donor retina 2 (J-L) and 3 (M-O). AAV potency measured by total GFP-positive cells / Total cells infected for donor 2 (U) and 3 (Y). Infection measured by GFP-fluorescence for donor 2 (V) and 3 (Z). GFP-positive cells per total cells in layer for donor 2 & 3 (W, AA). Tropism (GFP-positive cells in layer per Total GFP-positive cells) for donor 2 and 3 (X, BB). Retinal thickness between donors 1-to-3 at day 14 in culture (CC). Cells per layer in averaged image (DD). Each dot represents an individual image (P-BB). 90 images analysed donor 1, 30 images analysed donors 2 and 3 (CC and DD). ShY, ShH10Y445F; ONL, outer nuclear layer; INL, inner nuclear layer; GCL, ganglion cell layer; gc, genome copies. Scale bar: 20µm (A-O). Data are presented as mean ± SEM.

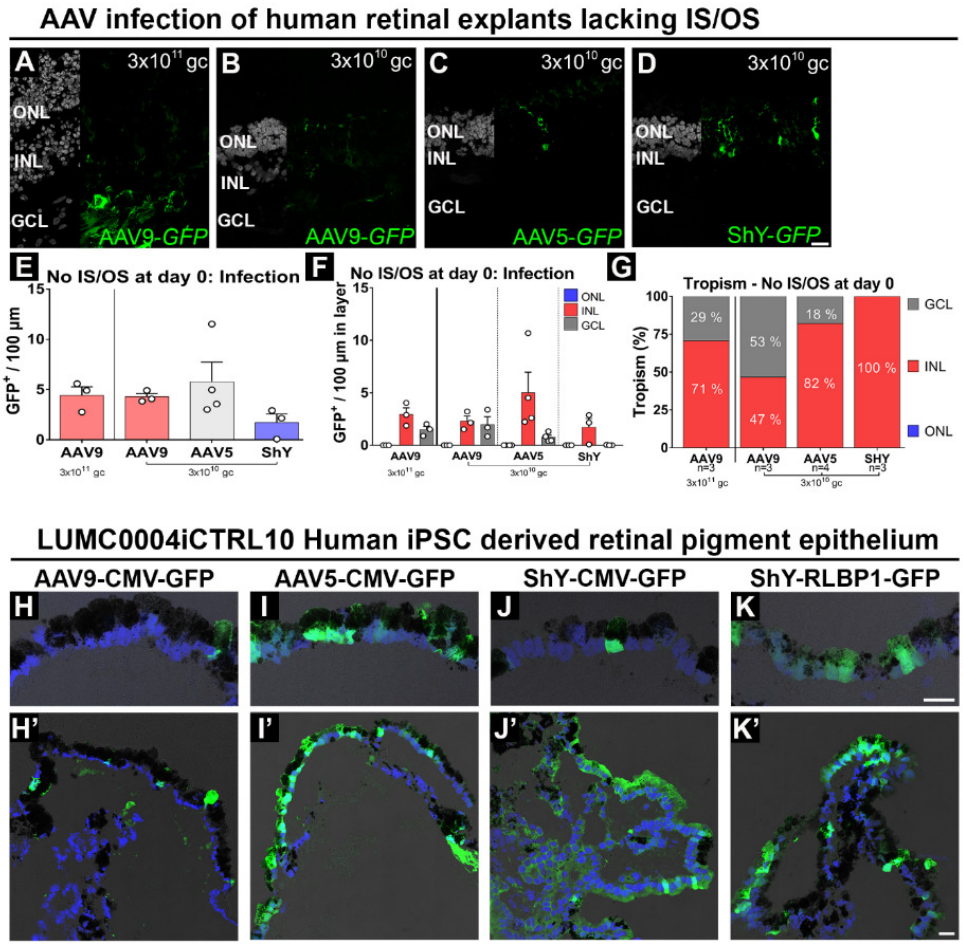

Figure S7. Human retinal explants lacking outer segments show no photoreceptor transduction. Related to Figure 6. Infection of human retinal explants missing outer segments with AAV9-CMV-*GFP* at $3x10^{11}$ gc (A) and $3x10^{10}$ gc (B), AAV5-CMV-*GFP* at $3x10^{10}$ gc (C) and ShH10Y445F-CMV-*GFP* at $3x10^{10}$ gc (D). Efficacy of transduction of retinal cell types was quantified by measuring the number of GFP-positive cells per 100 µm retinal length (E). GFP-positive cells per 100 µm retinal length in each layer (F). INL cells were mostly infected, and no photoreceptors were transduced by AAV9, AAV5 or ShH10Y445F (G). AAV9 at $3x10^{10}$ gc, $3x10^{11}$ gc and AAV5 at $3x10^{10}$ gc showed infection in the GCL. DAPI=grey. AAV-GFP=green. Each dot represents an individual donor (E, F), 10 images were analysed per donor (E-G). AAVs infect human iPSC derived retinal pigment epithelium. Related to Figure 7. LUMC0004iCTRL10 human derived retinal pigment epithelium is transduced at 10^{10} gc by AAV9-CMV-GFP (H, H'), AAV5-CMV-GFP (I, I'), ShH10Y445F-CMV-GFP (J, J') and ShH10Y445F-RLBP1-GFP (K, K'). DAPI=blue. Pigment=black. AAV-GFP=green. ShY, ShH10Y445F; ONL, outer nuclear layer; INL, inner nuclear layer; GCL, ganglion cell layer; gc, genome copies. Scale bar: (A-D, H-K, H'-K'), 20 µm. Data are presented as mean ± SEM.

Table S1. Antibody list and dilution used for immunohistochemistry and EM. Related to All Figures.

Antibody	Dilution	Manufacture	Catalogue Numbers
pH3	1:100	Millipore	06-570
Ki67	1:100	BD Biosciences	550609
p27kip1	1:200	Millipore	06-445
SOX9	1:250	Millipore	AB5535
Recoverin	1:500	Millipore	AB5585
Rhodopsin	1:500	Millipore	MAB5356
PAX6	1:100	DSHB	AB_528427
Islet1/2	1:200	DSHB	AB_2314683
Tuj1	1:200	Biolegend	801201
PKCα	1:250	BD Biosciences	610107
OTX2	1:200	Proteintech Europe	13497-1-AP
CRB1 AK2	1:200	Homemade	N/A
CRB2 EP13	1:200	gift from Pen Rashbass	N/A
CRB2 SK11	1:200	gift from Pen Rashbass	N/A
PALS1 SN47	1:200	Homemade	N/A
PAR3	1:100	Millipore	07-330
MUPP1	1:200	BD Biosciences	M98820
β-catenin	1:200	BD Biosciences	610153
p120-catenin	1:200	BD Biosciences	610134
N-Cadherin	1:250	BD Biosciences	610920
LHX2	1:200	Santa Cruz	sc-19344
peanut agglutinin (PNA)	1:200	Vector Lab	RL-1072
CD44	1:400	BD Biosciences	553132
PATJ	1:200	gift from André Le Bivic	N/A
SOX2	1:200	Santa Cruz	sc-17319
EAAT1 (GLAST)	1:100	Abcam	ab416
CRALBP	1:200	Abcam	ab15051
OPN1SW	1:200	Millipore	AB5407

Supplemental Experimental Procedures

Fetal human retinal tissue

Human fetal eyes at gestational age week 9 to 19 were collected from elective abortion material (vacuum aspiration) without medical indication, with signed informed consent and provided anonimised. In this study, "weeks of gestation" was used as determined by the last menstrual period (LMP).

Adult human retinal tissue

Patient anonymity was strictly maintained. All tissue samples were handled in a coded fashion, according to Dutch national ethical guidelines (Code for Proper Secondary Use of Human Tissue, Dutch Federation of Medical Scientific Societies). Post-mortem adult human

donor eye (from 56 to 88 years-old donors) were acquired within the LUMC and were processed within 24 hours after death.

Cell Culture and Retinal Organoid Differentiation

Three healthy lines (LUMC0004iCTRL10, LUMC0044iCTRL44, LUMC0080i CTRL12) and three male *CRB1* RP patient lines (LUMC0116iCRB09, LUMC0117iCRB01, LUMC0128iCRB01) were derived from skin fibroblast using polycistronic Lentiviral vectors [1]. The *CRB1* RP patient line LUMC0117iCRB01 also had the variant c.1892A>G (p.(His631Arg)) in the *RPGRIP1* gene, which was classified as a variant of unknown significance.

In brief, human iPSCs were collected and incubated with (±)blebbistatin in mTeSR medium overnight and transitioned from mTeSR/NIM-1 (3:1), to (1:1), and to (0:1) over the subsequent three days to form Embryoid Bodies (EBs) in floating culture. Floating EBs were plated onto Matrigel-coated wells from differentiation day (DD) 7 till DD28, with a change from NIM-1 to NIM-2 medium at DD16. At DD28 neuroepithelial rosettes are flushed loose from the matrigel using a P1000 pipet and are kept in floating culture in agarose coated plates from this point onwards. NIM-2 is used till DD41, RLM is used from DD42 to DD48, RLM-1 from DD49 to DD97, and RLM-2 from DD98 for long-term culture. Medium is changed as required, typically every other day from DD3 till DD33 and typically twice a week from DD41 onwards. Plates were checked for possible medium changes every other day. Neural Induction Medium 1 (NIM-1): 48.95 mL DMEM/F12 supplemented with 0.5 mL 100x N2 supplement, 0.5 mL 100x Minimum Essential Media-Non Essential Amino Acids (MEM NEAAs), 10 µL 10 mg/mL Heparin (Sigma). Neuronal Induction Medium 2 (NIM-2): 96 mL DMEM/F12 (3:1) supplemented with 2 mL 50x B27 Supplement, 1 mL 100x NEAA, 1 mL 100x antibiotic-antimycotic (10,000 units/mL of penicillin, 10,000 µg/mL of streptomycin, 25 µg/mL of amphotericin B). Retinal Lamination Medium (RLM): 107.25 mL DMEM/F12 (3:1) supplemented with 12.5 mL embryonic stem cell-qualified FBS, 2.5 mL 50x B27 Supplement, 1.25 mL 100x MEM NEAAs,1.25 mL 100x antibiotic-antimycotic (10,000 units/mL of penicillin, 10,000 µg/mL of streptomycin, 25 µg/mL of Amphotericin B), 0.25 mL taurine (100 µM final concentration). Retinal Lamination Medium 1 (RLM-1): RLM supplemented with 0.1 µL 10 mM retinoic acid (1 µM final concentration) per mL. Retinal Lamination Medium 2 (RLM-2): RLM supplemented with 0.05 µL 10 mM retinoic acid (0.5 µM final concentration) per mL.

Sequence validation on patient mutations in the *CRB1* gene

DNA of retinal cells were extracted with the DNeasy Blood & Tissue Kit (QIAGEN) from *CRB1* RP patient retinal organoids (LUMC0116iCRB09, LUMC0117iCRB01, LUMC0128iCRB01). Exon 6 was PCR amplified (Forward primer: TTTGAGGGCGATGGCTTCCT. Reverse primer: TGAGGCATGGCACTCCTAGC).

Exon 9 was PCR amplified (Forward primer: TGAACAAAATTACTTAAATTCTG TGAG. Reverse primer: TCCTCCATGCAAACAGGGGT). The samples were then purified (QIAquick PCR Purification) and then Sanger sequenced. Exon 6 was Sanger sequenced in forward and reverse direction:

Forward primer: TAATCAGTCAAAGGTGCTTCTGTT

Reverse primer: CTCTCAGACAGTTGGGGCCT

Exon 9 was sequenced in forward and reverse direction:

Forward primer: TGAACAAAATTACTTAAATTCTGTGAG

Reverse primer: TGTACTTAGACACCCTTGCAG)

The electropherograms were analysed in Snapgene Viewer (Version 3.2) and aligned to Exon 6 and Exon 9 extracted from the *CRB* gene region chromosome 1: 197,268,278-197,478,455 (ENSG00000134376 GRCh38).

Immunohistochemical analysis

Adult human donor retina, human fetal retina, hiPSC-derived retinal organoids were incubated for 30 minutes in 4% paraformaldehyde in PBS for fixation and 15% and then 30% sucrose in PBS for cryo-protection. Finally, retina were orientated, embedded in Tissue-Tek, frozen and stored at -20°C. Sections of 8-10 µm were made with a Leica CM1900 cryostat (Leica Microsystems). Sections for immunohistochemistry were blocked for 1 hour in 10% normal goat serum, 0.4% Triton X-100 and 1% bovine serum albumin (BSA) in PBS, incubated in a moist-chamber overnight at 4°C (Table S1) diluted in 0.3% normal goat serum, 0.4%Triton X-100 and 1% BSA in PBS. After rinsing in PBS, the sections were incubated for 1 hour with complementary conjugated secondary antibodies (Table 1) and rinsed in PBS again. Sections were mounted in Vectashield HardSet DAPI mounting media (Vector Laboratories). A Leica TCS SP8 confocal microscope were used for Image acquisition. Image analysis and processing were carried out using ImageJ and Adobe Photoshop CC2014, respectively.

Electron microscopy

In brief, 40 µm thick sections were incubated with the appropriate first antibody for 48 h (Table 1), then incubated with appropriate secondary (anti-Rabbit or anti-Mouse) peroxidise anti-peroxidase (PAP) for 2h, then developed in a 2,2-diaminobenzidine solution containing 0.03% H_2O_2 for 4 min and then the gold substitute silver peroxidise method applied. Sections were embedded in epoxy resin, ultrathin sections made and examined with an electron microscope (Microscope: FEI Tecnai T12 Twin Fei Company, Eindhoven, The Netherlands; Camera: OneView, Gatan) operating at 120 kV. Overlapping images were collected and stitched together into separate images as previously described [2]. At least two independent

samples were analysed per time point for human fetal eyes and human iPSC-derived retinal organoids and RPE.

Generation and purification of the viral vectors

Briefly, pAAV2-*eGFP* plasmids were co-transfected with the pHelper and pAAV9, pXX2-ShH10Y445F, or pDP5rs capsid plasmid into HEK293T cells to generate AAV9, ShH10Y445F or AAV5 viral particles. After benzonase treatment, the lysates were ultra-centrifuged onto an iodixanol density gradient and concentrated on Amplicon spin columns (100 kDa, Millipore). All viral titers were determined by quantitative PCR and all viral stocks with titers around 1×10^{13} genome copies per ml were stored at −80°C.

In vitro transduction of human donor retina and human induced pluripotent stem cell derived retinal organoids

1) In brief, 3-6 6 mm punches of human donor retina were dissected in cold HBSS (Sigma) within 24 hours after death. Whatman™ paper was placed on the ganglion cell side of each punch. Punches were then placed, photoreceptor side down, on Millicell Cell culture Inserts (Millipore, PICM01250) and placed into a 24 well plate with 300 µL of explant medium per well. After that, 50 µL of explant medium with the desired titre of a viral vector ($3x10^7$, $3x10^9$, $3x10^{10}$ or $3x10^{11}$ gc) was added to Whatman™ paper for 48 hours, and medium changed every other day until day 14. Explant medium: 300 µL 50X B-27 Supplement (Invitrogen), 150 µL 100X N-2 Supplement (Invitrogen), 30 µL 50 mM Taurine, 120 µL 200 mM L-glutamine, 150 µL 100 mM sodium pyruvate, 18.45 µL 1 mM N-Acetyl-L-cysteine, 150 µL 100X antibiotic-antimycotic (10,000 units/mL penicillin, 10,000 µg/mL streptomycin, 25 µg/mL Amphotericin B) in a final volume of 15 mL Neurobasal®-A medium (Invitrogen). 2) In brief, two retinal organoids were placed in 1%-agarose coated wells of a 96-well plate, and 50 µl of RLM-2 containing the 10^{10} gc of the AAV vector was added for 24 hours. A further 50 µL of RLM-2 only was added to the well for another 24 hours. The organoids were washed three times in PBS and replated in RLM-2 in a 24-well plate. The medium was then changed twice a week for 14 days post infection. Tissues were fixed, cryo-protected and frozen for further processing as described in: Immunohistochemical analysis.

Quantitative analysis of GFP fluorescence intensity and cell number

Quantitative analysis of GFP expression allowed for assessment of both AAV potency and tropism in human donor retina and hiPSC-derived retinal organoids. For the quantitative analysis of GFP expression, images were taken using a Leica TCS SP8 confocal microscope (Leica). Images were obtained at 40x magnification using identical acquisition settings, including laser intensity, and were saved at a resolution of 1024x1024 pixels. GFP expression profiles were measure in three ways: 1) GFP positive cells per total cells, 2) Mean grey value (Transduction profiles were analyzed by defining a region of interest (ROI) for the outer

nuclear layer, inner nuclear layer and ganglion cell layer for human donor material and a top nuclear layer and bottom nuclear layer for the hiPSC-derived retinal organoids), and 3) GFP-positive cells in layer per cells in layer. Tropism was measured as GFP-positive cells in layer (ONL, INL or GCL/Nerve Fiber Layer) per total GFP-positive cells. The Cell Counter plugin for ImageJ was used to quantify total cell number (counterstain: DAPI, LHX2, and SOX2) and total GFP positive cell number for each ROI. The number of GFP positive cells for each ROI was divided by the total number of cells for each ROI to obtain the percentage of transduced cells. Fluorescence images were also analysed by calculating the mean grey value (MGV), corrected for area and background levels of fluorescence, for each ROI using ImageJ software. 6-mm harvested retinal explant punches were sectioned at 90 degree angle [3]. This allows to assess the AAV transfection on the whole retina stretch of 6-mm retinal explant punch. Edges or otherwise damaged areas where not used for image acquisition. Between 3-6 different sections from at least three different human donor retina or hiPSC-derived retinal organoids were used for quantification of mean grey value or cell counting's (>900 µm in retinal length. 3-5 images per organoid and 10 images for adult donor retina).

Supplemental References

1. Warlich, E.; Kuehle, J.; Cantz, T.; Brugman, M.H.; Maetzig, T.; Galla, M.; Filipczyk, A.A.; Halle, S.; Klump, H.; Schöler, H.R.; et al. Lentiviral vector design and imaging approaches to visualize the early stages of cellular reprogramming. *Mol. Ther.* **2011**, *19*, 782–789.

2. Faas, F.G.A.; Cristina Avramut, M.; van den Berg, B.M.; Mieke Mommaas, A.; Koster, A.J.; Ravelli, R.B.G. Virtual nanoscopy: Generation of ultra-large high resolution electron microscopy maps. *J. Cell Biol.* **2012**, *198*, 457–469.

3. Buck, T.M.; Pellissier, L.P.; Vos, R.M.; van Dijk, E.H.C.C.; Boon, C.J.F.; Wijnholds, J. AAV serotype testing on cultured human donor retinal explants. In *Methods in Molecular Biology*; Boon, C.J.F., Wijnholds, J., Eds.; New York, NY: Humana Press: New York, NY, 2018; Vol. 1715, p. pp 275-288 ISBN 978-1-4939-7522-8.